

TRW REPORT NO. 14103-6003-R0-00

FINAL REPORT

**DEVELOPMENT OF LASER INSTRUMENTATION  
FOR  
PARTICLE MEASUREMENT**

JUNE 1971

prepared by

**B. J. MATTHEWS and R. F. KEMP**

CONTINUATION OF EPA CONTRACT CPA 70-4

**TRW**  
SYSTEMS GROUP

ONE SPACE PARK • REDONDO BEACH • CALIFORNIA

OFFICIAL USE ONLY

Final, interim and monthly reports submitted under this contract contain information and statements which are preliminary and represent only the state of the information developed as of the reporting date. This information is also subject to review and critique by EPA personnel before release outside of EPA. To prevent inappropriate dissemination of information which could be misinterpreted and/or misleading, you are asked to regard these reports strictly as internal working documents and treat them accordingly. You are requested to observe the following guidelines:

- (1) Use the reports for information and coordination purposes only.
- (2) Do not discuss the reports or the information contained in them with persons outside of EPA.
- (3) Refer all inquiries relating to the reports to the Project Officer.
- (4) Provide comments to the Project Officer for his use in managing the contract.

TRW REPORT NO. 14103-6003-R0-00

FINAL REPORT

**DEVELOPMENT OF LASER INSTRUMENTATION  
FOR  
PARTICLE MEASUREMENT**

JUNE 1971

prepared by

**B. J. MATTHEWS and R. F. KEMP**

CONTINUATION OF EPA CONTRACT CPA 70-4

**TRW**  
SYSTEMS GROUP

ONE SPACE PARK • REDONDO BEACH • CALIFORNIA

## FOREWORD

This report summarizes analytical and experimental work accomplished under Modification No. 7 to the Environmental Protection Agency's Contract CPA 70-4, dated 20 April 1970. Submittal of this report is in accordance with provisions of the referenced contract.

Technical direction and administration of the program by the Environmental Protection Agency was provided initially by Dr. Frederic C. Jaye, and later in the program, by Mr. Robert M. Statnick. The TRW Project Manager was Mr. B. J. Matthews. TRW staff engineer, Mr. R. F. Kemp, was responsible for developing and demonstrating the laser-illuminated synchronous detection system used at the Shawnee Power Plant during field tests. Mathematical modeling of laser beam scattering together with basic particle scattering measurements was accomplished by Dr. L. O. Heflinger of TRW's Systems Group Research Staff. Dr. R. F. Wuerker of the Systems Group Research Staff developed the holographic methods for recording both side and back scattering of the pulsed ruby laser beam. The authors are also indebted to Drs. Wuerker and Heflinger for the use of the TRW Chlorophyll dye cell used in the successful demonstration of holography of side and back scatter over extended distances.

## CONTENTS

	Page
1. INTRODUCTION AND SUMMARY .....	1
1.1 Background .....	1
1.2 Summary of Results .....	2
2. ANALYSIS .....	4
2.1 Scattering Relationships .....	4
2.2 Supporting Laboratory Tests .....	9
2.3 Particle Microscopy .....	19
3. EXPERIMENTAL EQUIPMENT .....	32
3.1 Ruby Laser Holocamera .....	32
3.2 Synchronous Detector .....	36
4. RESULTS .....	40
4.1 Unit 10 Transmission Measurements .....	40
4.2 Unit 10 Light Scattering Experiments .....	42
5. CONCLUSIONS .....	60
6. RECOMMENDATIONS .....	63
REFERENCES .....	64

## ILLUSTRATIONS

	Page
1. Schematic diagram of probing beam and scattered light geometry .....	6
2. Detail of beam intersection .....	7
3. Plot of the concentration function, $y = xe^{-x}$ .....	8
4. Schematic diagram of apparatus used for scattering and transmission measurements .....	10
5. Transmission of laser beam as a function of concentration for Unit 10 flyash and flyash-limestone mixtures .....	11
6. Ninety degree scattering of laser beam as a function of concentration for Unit 10 flyash and flyash-limestone mixtures .....	13
7. Straight path transmission versus $90^{\circ}$ scattering for mechanically and electrostatically precipitated flyash samples with and without limestone .....	14
8. Polar plot of scattering intensity for Unit 10 electrostatically precipitated flyash-limestone mixture .....	15
9. Polar plot of scattering intensity for Unit 10 electrostatically precipitated flyash dust .....	16
10. Polar plot of scattering intensity for Unit 10 mechanically collected flyash dust .....	17
11. Scanning electron microscope (SEM) photograph of flyash-limestone mixture .....	20
12. SEM micrograph (300X) of broken flyash sphere .....	21
13. SEM micrograph of broken flyash sphere of 80 micron broken sphere .....	22
14. Extreme enlargement of SEM micrograph of hollow sphere ....	23
15. SEM micrograph of fractured flyash sphere .....	24
16. SEM micrograph of flyash particle with hole melted in surface .....	26
17. SEM micrograph of second flyash sphere with hole melted in surface .....	27

# ILLUSTRATIONS (Continued)

	Page
18. Transmission micrograph (400X) of 80 micron diameter particle .....	29
19. Six micrographs of 150 micron particle showing progressive disintegration of structure .....	30
20. Micrograph (160X) of small 50 micron particle imbedded in larger 140 micron flyash particle .....	31
21. Schematic diagram of holographic arrangement for recording ruby laser back scattering .....	33
22. Schematic diagram of holographic arrangement to record side scattering of ruby laser beam .....	35
23. Schematic diagram of laser illuminated synchronous detector	37
24. Photomultiplier tube and focusing telescope assembly .....	38
25. Schematic diagram of setup for transmission measurements at elevation 392 of the Unit 10 superheater region .....	40
26. Schematic diagram of setup for scattering measurements at elevation 376 of the Unit 10 boiler .....	43
27. Relative locations from which scattered light measurements were made .....	46
28. Strip chart record of laser light transmission across Unit 10 superheater at elevation 392, on 16 March 1971 .....	52
29. Strip chart record of 90 degree scattering at elevation 376 on 18 March 1971.....	54
30. Strip chart record of 125 degree scattering at elevation 376 on 18 March 1971 .....	55
31. Strip chart record of 115 degree scattering at elevation 376 on 18 March 1971 .....	56
32. Schematic diagram of proposed three-beam holocamera design for use at the Shawnee Unit 10 boiler .....	59

## LIST OF TABLES

		Page
I.	Transmission measurements, Unit 10 superheater, elevation 392, 16 March 1971 .....	41
II.	Values of $n$ and $mfp$ for transmission data, Unit 10 superheater, elevation 392, 16 March 1971 .....	42
III.	Tabulation of results of "single point" method using Eq. (6) to solve for transmittance with and without limestone, and a list of the ratios of transmittance with limestone to transmittance without limestone ....	47
IV.	Calculation of the scattering fraction $\beta$ , assuming $mfp = 66$ inches .....	49
V.	Calculation of the scattering fraction $\beta$ , assuming $mfp = 55$ inches ... ..	49
VI.	Calculations of the scattering fraction $\beta$ using the "two-point" method .....	51



## 1. INTRODUCTION AND SUMMARY

### 1.1 BACKGROUND

This report summarizes recent developments in laser-illuminated instrumentation for measuring particulate density distributions in an operating coal-fired steam boiler. The development work, sponsored by the Environmental Protection Agency (EPA), is part of an ongoing program at TRW Systems Group to characterize limestone particle distributions injected into a boiler to remove sulfur oxide from the combustion gases. Field tests in this program were conducted at the Tennessee Valley Authority's (TVA) Shawnee Power Plant where the full scale dry limestone program is being evaluated on one of ten identical 140 megawatt boilers.

This report is the third in a series by TRW covering development of laser instrumentation for particulate visualization and measurement.\* The previous studies are reported in References 1 and 2; however, a brief review of the highlights of this past work is useful as an introduction to the present investigation.

Initial work under this contract was concerned with applying single beam (Gabor) pulsed ruby laser holography to the recording of particulate over extreme distances. Although this technique was not ultimately used at the boiler, Gabor holography was extended into an area never before explored; namely, recording distributed phenomena across distances up to 50 feet.

Two-beam ruby laser holography was successfully utilized at the Shawnee Unit 10 boiler to record particulate clouds and obtain spatial information as well as qualitative details of the limestone clouds in the presences of flyash backgrounds.<sup>1</sup> This was by the forward scattering method. Subsequently, a three-beam scattered light holography technique was devised to acquire quantitative particle number density data directly from the reconstructed holographic areal real image.<sup>2</sup> Means were also developed to holographically record ruby laser back scatter by particulate thus adding more flexibility to the basic technique. The latter method, first described in Reference 2, was accomplished in a preliminary manner and served as a basis for the present work.

Earlier work involving transmission holography of low angle forward scattering by particulate in the Unit 10 boiler necessitated using two directly opposed ports in the boiler walls. The absence of opposed ports in the region of interest (elevation 376) precluded transmission studies. It was desired, therefore, to investigate the feasibility of recording laser back scatter through a single port, or recording side scatter by

---

\* EPA Contract CPA 70-4

the use of a combination of two of the several existing ports at this elevation. The objective of the present work then, was to determine if limestone dust in the presence of a flyash background could be recorded holographically via back or side scattering of a ruby laser beam.

## 1.2 SUMMARY OF PRESENT WORK

To investigate the feasibility of making holograms of side (approximately 90 degree) or back scattering of a ruby laser beam, a mathematical model was first derived. This model (Eq. 6, in Section 2.1) relates the following factors which describe the "transmittance" of scattered light: (1) geometric relationships of the incident and scattered (received) beams; (2) scattering efficiency of the particulate; (3) angular dependence of the scattering; and, (4) the particulate concentration dependence. The relationship of these four factors gives the transmittance along the scattering path from the laser to a detector (hologram, photomultiplier tube, etc.), and allows analysis of experimental measurements.

Development of a mathematical model of the scattering was augmented by laboratory tests to: (1) assess variations in scattering efficiency between Shawnee Unit 10 flyash and flyash-limestone mixtures; and, (2) determine angular dependence of the scattering intensity for both types of particulate. The tests showed that there was less than a factor of two difference in the scattering efficiency between flyash and mixtures of flyash and limestone dust. Intensity of the scattering was predominantly in the low angle forward direction with a smaller lobe in the back scatter direction. Side scattering ( $\sim 40$  to  $160$  degrees) was the least intense. It was a factor of  $\sim 10^3$  less than the intensity of forward scatter, and between 10 and 20 times less than back scatter intensity.

In addition to the scattering measurements, particle microscopy studies were extended beyond those reported in Reference 2, with the aid of a scanning electron microscope (SEM). This work revealed that in some instances at least, smaller particles are encapsulated in larger flyash spheres during the boiler combustion process. Determination of the mass fraction of encapsulated particles was not attempted.

Early in the program, it was decided to change the scope of work to include preliminary scattering measurements at the Shawnee Unit 10 boiler.\* Original plans called only for straight path transmission measurements at elevation 392 of the Unit 10 superheater. Ultimately, scattering holograms were contemplated for elevation 376 (Plane A-A) and

---

\* Modification No. 7 to Contract CPA 70-4.

there were no opposed ports at this elevation with which to measure transmittance. To assess the feasibility of recording back and side scattered light holograms, it was also necessary to make preliminary scattering measurements at this lower elevation. Subsequently, transmission measurements were made across the superheater (elevation 392) and scattering measurements were made at Plane A-A during the period 16 to 18 March 1971.

The transmission measurements were made in the absence of any limestone injection and indicated that average flyash particle densities varied between 4000 and 4600 particles/in<sup>3</sup>.

Existing port locations were used at elevation 376 to make scattering measurements both with and without limestone injection into the boiler, on 17 and 18 March 1971. Measurements were made at scattering angles of 90, 115 and 125 degrees. The measuring apparatus consisted of a continuous wave helium-neon gas laser, a chopper to convert the incident laser beam into a 750 Hz a.c. signal, a telescope and photomultiplier assembly to observe and measure the intensity of the scattering signal, and a lock-in amplifier. The output signals from the photomultiplier and the lock-in amplifier were recorded on a two-channel strip chart recorder. This assembly of components was termed a synchronous detection system.

A factor of between 1.3 and 2.4 increase in the amount of scattered light was measured during periods of limestone injection. The traces exhibited a high degree of noise. Analysis of the measured data using the mathematical model led to inconclusive results with regard to determining particle concentrations. Differences in particle concentration between conditions with and without limestone injection could not be ascertained. They were obscured by signal noise and uncertainties in geometric and scattering factors in the mathematical model.

Calculations based upon the measured scattering intensities at elevation 376 indicate that pulsed ruby laser holography of particle back scatter may be feasible. The depth of field of the holograms will probably be limited to a distance of about six feet inside the boiler.

The scattering measurements at elevation 376 were also analyzed to determine particle flow field dynamic characteristics. This analysis indicated that limestone distribution at this elevation does not appear spatially or temporally uniform. Random variations in signal intensity and frequency were noted during periods of limestone injection.

## 2. ANALYSIS

This section is concerned with development of a model for scattering by flyash particles of a light from a probing laser beam. The analysis was done by Dr. L. O. Heflinger of the TRW Systems Group Research Staff (SGRS). The work was in preparation for a test program at the Shawnee Unit 10 boiler (Section 4.2). In addition, laboratory scattering measurements were made by Dr. Heflinger in support of the analysis and subsequent Unit 10 data reduction and evaluation. Also included in this section are the results of supporting particle microscopy work. This is an extension of previous microscopic studies of flyash.<sup>2</sup>

### 2.1 SCATTERING RELATIONSHIPS

The following is a brief summary of scattering relationships between the probing laser light and Unit 10 flyash particles. The scattering relationships led to a mathematical formula which gives the intensity of scattered light in terms of particle concentration and the geometry of the optical configuration. In the following discussion, let

$n$  = the number of particles per unit volume.

$\sigma$  = the geometric cross section area of a particle.

For a spherical particle,  $\sigma = \pi D^2/4$ , where  $D$  is the diameter of the particle. In the scattering formulas, it is the product  $n\sigma$  which enters the formulas. From TVA data on Shawnee Unit 10 particle size distribution, it has been determined by integration that the effective particle diameter is  $40\mu$  ( $40 \times 10^{-6}$  m), giving an effective  $\sigma$  of:

$$\begin{aligned}\sigma_{\text{eff}} &= \pi/4 (40 \times 10^{-6})^2 \\ \sigma_{\text{eff}} &= 1.26 \times 10^{-9} \text{ m}^2.\end{aligned}\tag{1}$$

If this effective value is used, the value of  $n$  obtained from the formulas will be the total particle concentration, counting all sizes of particles.

Note that  $4 n\sigma$  is the total surface area of the particles per unit volume, for spherical particles. Thus, the light scattering experiments can be interpreted as measuring the particle surface area per unit volume directly. It can be shown that the value of  $n\sigma$  determined by experiment gives the total particle surface area per unit volume essentially independent of the particle size distribution.

### Transmission Measurements

The number of particles per unit of volume may be obtained by measuring the transmitted light through a scattering medium. In this

case, let

$L$  = length of path through the scattering medium.

$T$  = transmittance of this path

$$= \frac{\text{intensity of output beam}}{\text{intensity of input beam}}$$

Then for a uniform scattering region

$$T = e^{-2n\sigma L} \quad (2)$$

This can be rewritten

$$n\sigma = \frac{1}{2L} (-\ln T)$$

or,

$$n\sigma = \frac{1}{2L} \ln \frac{1}{T} \quad (3)$$

If the scattering is not uniform throughout the region, the value of  $n\sigma$  obtained is the average over the path  $L$ . The coefficient of  $L$  in Equation (2) is the extinction coefficient and has the dimensions of an inverse distance. Hence, the distance  $1/2n\sigma$  is characteristic of the scattering medium, and is the distance over which the intensity of transmitted light is attenuated by the factor  $e = 2.718...$ . Hence, a given photon has about a 37 percent probability of traversing this distance within the medium before encountering a scattering particle. We take the liberty of calling this distance "mfp" and note that it has nothing to do with the mean-free-path of kinetic theory. This distance may be calculated from a transmission measurement by rewriting Equation (2) again:

$$\text{"mfp"} = \frac{1}{2n\sigma} = \frac{L}{-\ln T} \quad (4)$$

### Scattered Light Measurements

At most planes of interest within the Unit 10 boiler, directly opposed ports for transmission measurements do not exist. Therefore, one would like to estimate local particle concentrations based upon low angle back scatter measurements where only a single viewing port is required. An alternative is the measurement of side scatter intensities provided two ports are available which allow intersecting optical paths.

For the measurement of direct back scatter or of side scatter, a number of geometric factors must be determined. The relationship of the probing and scattered beams is shown in the Figure 1 sketch. In this sketch,  $\theta$  = angle of observation ( $\theta = 0$  is looking into the beam).

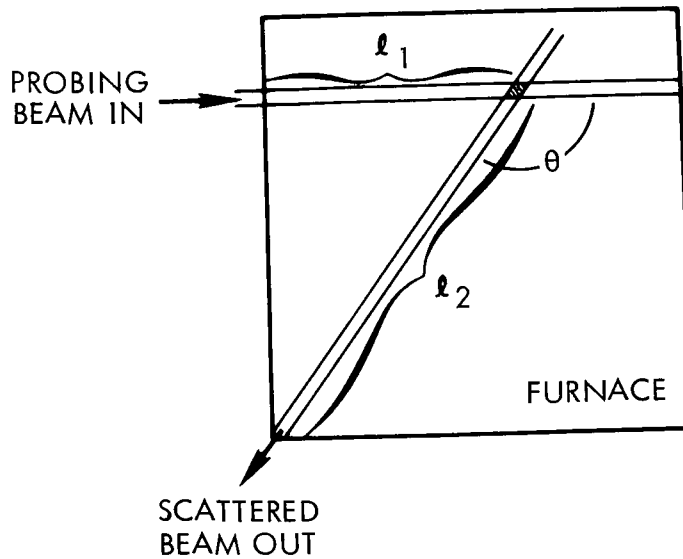


Figure 1. Schematic diagram of probing beam and scattered light beam geometry.

The small volume element from which light is scattered into the receiving optical system is defined by the intersection of two beams. One is the laser beam and the other may be called the viewing beam. A small aperture (approximately 1 mm diameter) is placed at the focal point of the telescope objective lens. Light passing through this aperture falls on the photomultiplier tube. Consequently, the image of this aperture within the scattering volume determines the axial position and diameter of the viewing beam. It is convenient, though not exact, to approximate the resulting scattering volume element as the intersection of two cylinders having intersecting axes at an angle  $\theta$ . If the diameter of the viewing beam  $w$  at the scattering point is larger than the laser beam, the situation is particularly simple: If  $S$  equals the cross-section area of the laser beam, then the fraction of light incident on the scattering volume element which each particle removes is  $\sigma/S$ . The total number of particles  $N$  in the volume element is  $n$  times the volume of the element or

$$N = nwS/\sin \theta$$

and the total fraction of light removed from the beam within the volume element is  $N\sigma/S = n\sigma w/\sin \theta$ . Of this light, a fraction,  $\beta$ , is scattered

(we assume here) uniformly in all direction. The scattered light fraction is thus,

$$\frac{P_{out}}{P_{in}} = \frac{w}{\sin \theta} \beta n \sigma \quad (\text{steradian}^{-1})$$

Figure 2 shows a detailed view of the intersection of the laser beam and the viewing beam in the case where the telescope aperture is a slit and the image of this slit has width  $w$  and thickness less than the diameter of the laser beam. In this, and other similar cases, the fraction  $\alpha$  may be used with  $w$  to give the effective length of the laser beam in the scattering volume element. The fraction  $\alpha$  is chosen so that  $w\alpha/\sin \theta$  is equal to the actual volume seen by the telescope. The solid angle subtended at the scattering volume element by the receiver optics if  $\Gamma = \pi r^2/R^2$  (steradian) where  $r$  is the radius of the entrance pupil and  $R$  is the distance from the scattering volume to the telescope. Finally, the total path length for absorption is  $L = \ell_1 + \ell_2$ , so that the total transmittance for the system is given by

$$T = \Gamma \left( \frac{1}{4\pi} \right) \frac{w\alpha}{\sin \theta} \beta n \sigma e^{-2n\sigma L}$$

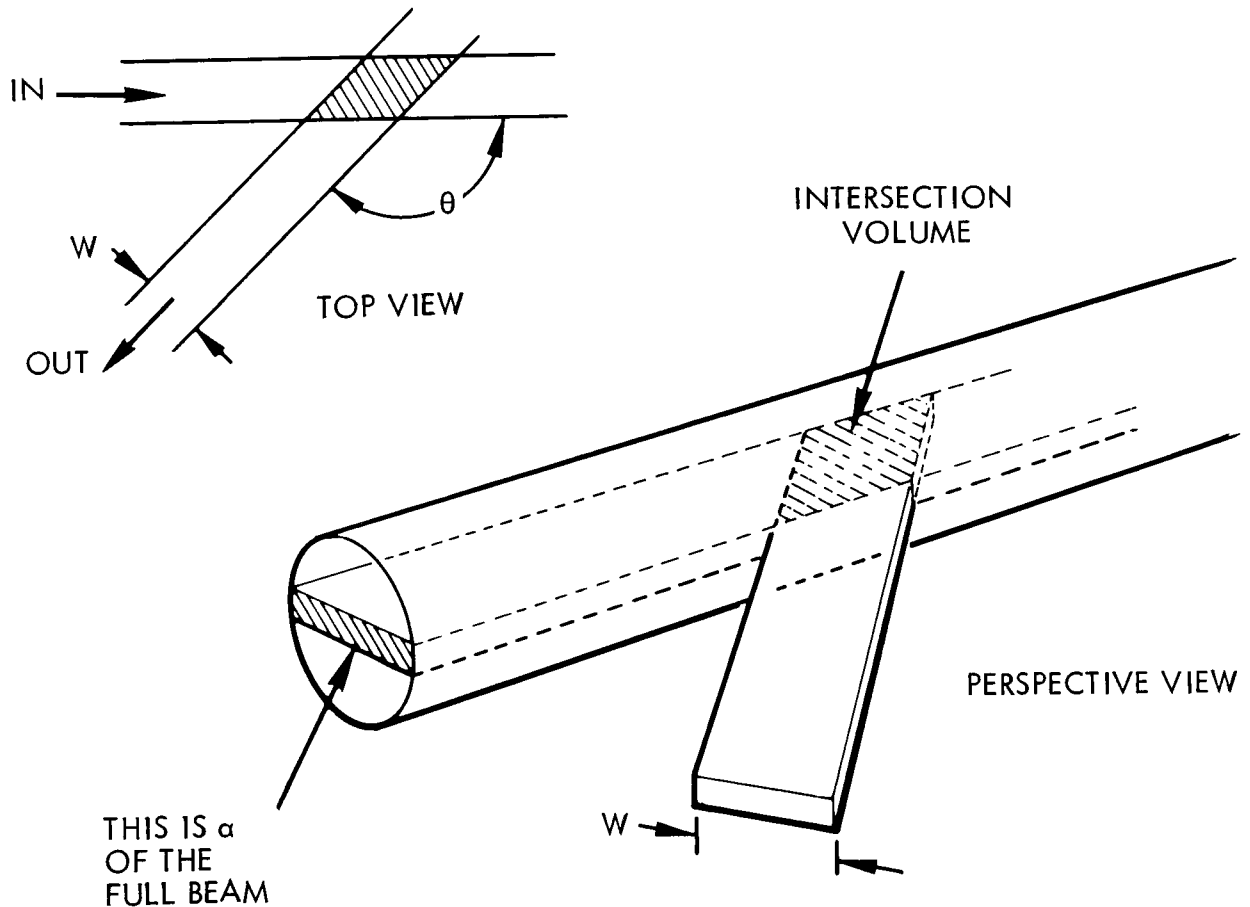


Figure 2. Detail of beam intersection

This can be rewritten as

$$T = \frac{\Gamma}{8\pi L} \frac{w\alpha}{\sin \theta} \beta (2n\sigma L) e^{-2n\sigma L} \quad (5)$$

in order to obtain a factor involving the product  $n\sigma$  which has the form

$$y = xe^{-x} \quad , \quad x = 2n\sigma L$$

and which may be called the concentration function. This function is plotted in Figure 3, and may be used to predict the behavior of the transmittance of the system for a given path length  $L$  as the (uniform) number density is increased from zero. For low values of particulate loading, the received intensity is nearly proportional to number density. However, as  $n$  increases to the point where  $1/2n\sigma = L$ , the intensity reaches a maximum. Beyond this point, extinction proceeds more rapidly than scattering fraction, and the received intensity decreases as the number density increases. However, one should not overlook the fact that if the particulate loading is highly non-uniform, scattering of light is proportional to the number density within the scattering volume element, while attenuation is related to average number density over the path length  $L$ . In general, the scattering of light is not uniform, so that the angular dependence is not simply  $1/4\pi$  as assumed above, but is given by a function  $f(\theta)$  such that over a sphere,  $\int f(\theta)d\theta = 1$ .

On the basis of these parameters and considerations, the following formula gives the transmittance via the scattering path from the laser to the detector, and will serve as a mathematical model for analysis

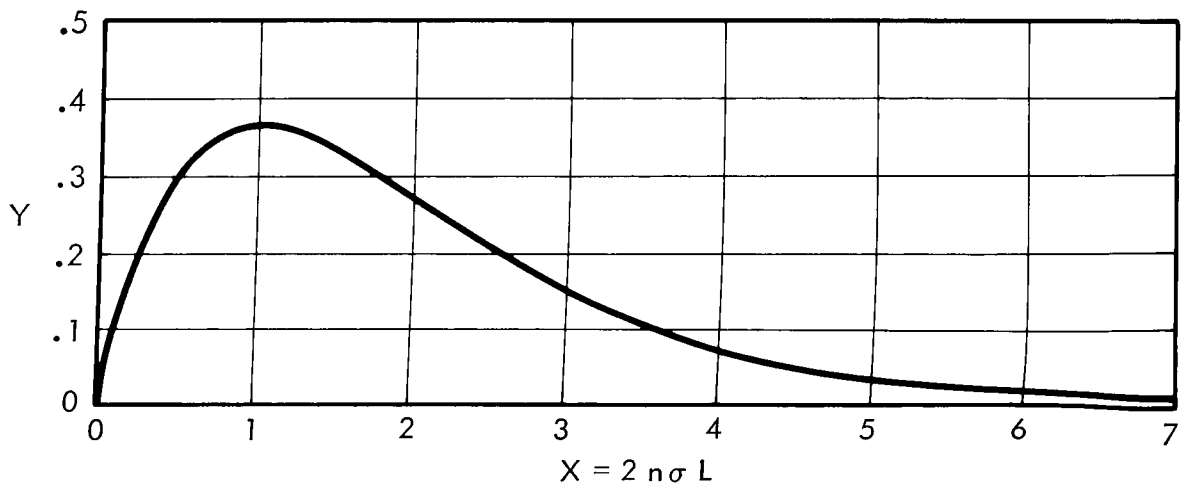


Figure 3. Plot of the concentration function,  $y = xe^{-x}$ .



of experimental results.

$$\tau = \underbrace{\frac{\Gamma W \alpha}{8\pi L}}_{\text{Geometric Factors}} \cdot \underbrace{\beta}_{\text{Particle Scattering Efficiency}} \cdot \underbrace{\frac{f(\theta)}{\sin \theta}}_{\text{Angular Dependence}} \underbrace{(2n\sigma L)e^{-2n\sigma L}}_{\text{Concentration Dependence}} \quad (6)$$

The following section describes some laboratory experiments in which measurements were made of the angular dependence of the scattering fraction. In as much as this turned out to be a slowly varying function for the range of angles used in scattering measurements within the Unit 10 boiler at the Shawnee Power Plant, Equation 6, above, was used in the data analysis.

## 2.2 SUPPORTING LABORATORY TESTS

Laboratory measurements were made to assess particle scattering efficiency and angular dependence terms in Eq. (6) for flyash and mixtures of flyash and limestone. Samples were obtained from both the Unit 10 mechanical collector and electrostatic precipitator.

A schematic diagram of the test apparatus is shown in Figure 4. A beam from a 1.6 milliwatt helium-neon gas laser is directed through a scattering cell. The light scattering cell contains two flat windows through which the laser beam passes. The rear portion of the cell is frosted to prevent reflections. The output of the laser and the intensity of the light after transmission through the scattering cell are monitored with silicon detectors as shown in the schematic. The laser silicon detectors and scattering cell are mounted on a heavy duty rotating azimuth head. The telescope and photomultiplier assembly used to measure the scattered light remain stationary.

Alignment of the telescope onto the laser beam passing through the scattering cell is accomplished using a mirror with an aperture located at the focal point of the 2 inch diameter, 8 inch focal length objective of the telescope. An eyepiece mounted normal to the telescope axis allows the observer to accurately align the laser beam scatter in the telescope aperture. The photomultiplier then receives the maximum scattering signal.

Measurements of the light transmission and scattering intensities of flyash and of flyash-limestone mixtures were made by suspending the appropriate particulate in water. A mechanical agitator was used to keep the particles in suspension. Measurements were made for different particulate concentrations as well as for changes in the scattering

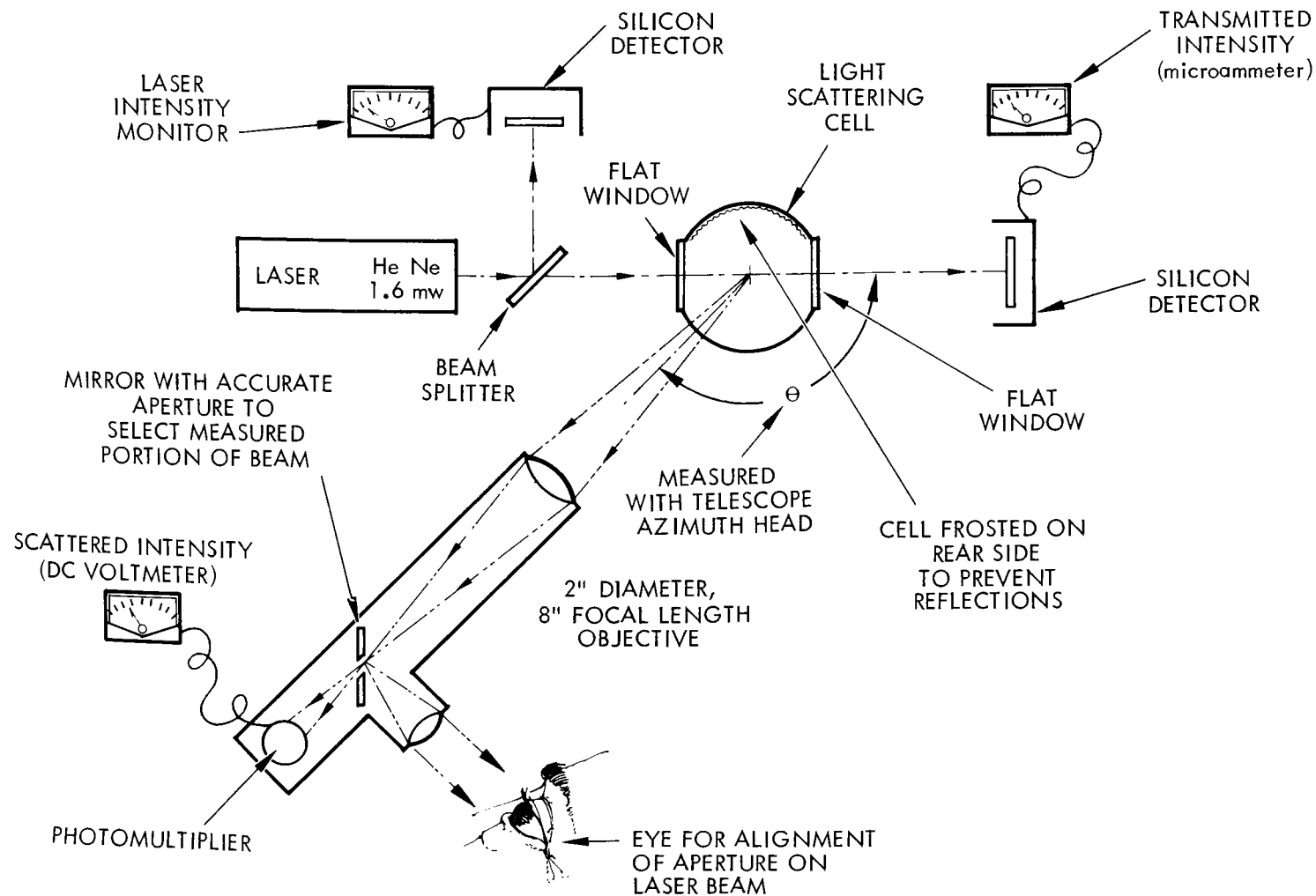


Figure 4. Schematic diagram of apparatus used for scattering and transmission measurements.

angle,  $\theta$ . The angle  $\theta$  was varied within the limits of the apparatus setup resulting in measurements from  $\theta = 6$  degrees to  $\theta = 174$  degrees ( $\theta = 180$  degrees represents back scatter while  $\theta = 0$  degrees is transmitted light).

### Transmission Measurements

Transmission data for various concentrations of both electrostatically precipitated and mechanically separated Unit 10 flyash and flyash-limestone mixtures are plotted in Figure 5. The transmission path was 35.5 mm. The data cover a range of volumetric concentrations of from 0 to 6. The unit of volumetric measure is arbitrary and termed a "millispoon" (ms). For the mechanically separated dust, one ms contains  $6.4 \times 10^{-3}$  grams (dry). One ms of electrostatically precipitated dust contains  $5.5 \times 10^{-3}$  grams. Thus at a concentration of 4 with mechanically separated flyash, the density would be  $(6.4 \times 10^{-3}) \text{ g/ms} \times (4 \times 10^{-2}) \text{ ms/cc} = 2.56 \times 10^{-4} \text{ g/cc}$ . Similarly, at the same concentration the electrostatically precipitated flyash density would be  $2.20 \times 10^{-4} \text{ g/cc}$ , etc.

The curves of Figure 5 show that at higher concentrations of particulate, there is an increase in the attenuation of the transmitted laser beam. Further, for equivalent concentrations, the light attenuation is greater for suspensions of electrostatically precipitated dust than for mechanically separated particulate. This is due to the smaller size distribution of the electrostatically precipitated flyash. For example, in one analysis, approximately 55 percent of the dust

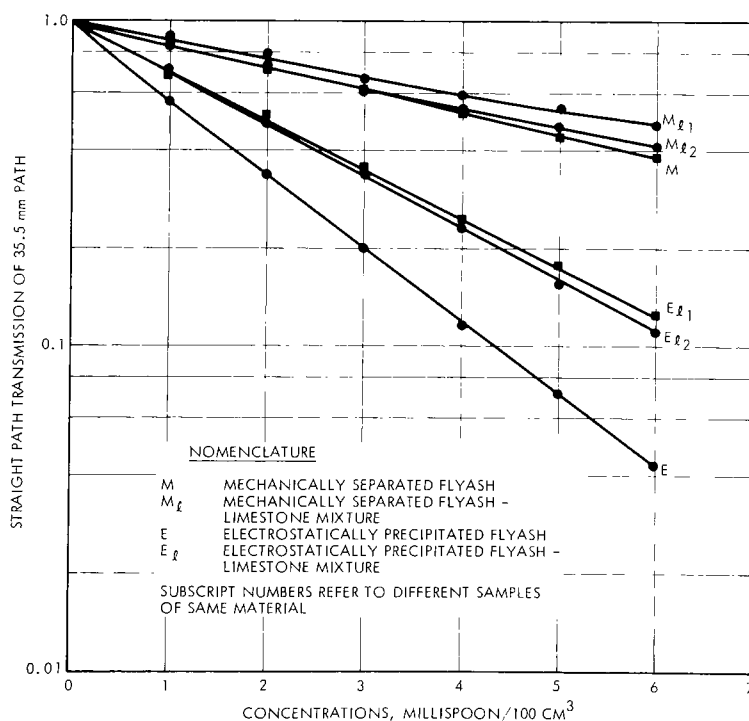


Figure 5. Transmission of He-Ne gas laser light beam as a function of concentration for Unit 10 flyash and flyash-limestone mixtures.

collected from the Unit 10 electrostatic precipitator was found to be less than 10 microns in size.<sup>3</sup> Conversely, only 7-10 percent of the dust collected by the mechanical separator on Unit 10 was less than 10 microns.<sup>3</sup> The significant increase in fines in the electrostatic precipitator flyash results in a corresponding increase in the total particulate surface area intercepted by the transmitted laser beam. The expression for light transmission through a scattering medium is  $T = \exp(-n\sigma\ell)$  where  $n\sigma$  is the product of the number of particles and the average particle scattering cross-section over the path length  $\ell$ . The product  $n\sigma$  is also proportional to the total surface area of the particles. Therefore, as the total particulate surface area increases, more light in the beam is intercepted and the beam attenuation is increased.

Of greater significance to the present work, however, is that there generally appears to be little difference in the light attenuation characteristics between flyash samples containing limestone dust and those without limestone. This is seen in Figure 5. Some deviation does occur between the samples with and without limestone for the electrostatically precipitated dust, but only at very high concentrations. In other words, one could not expect to readily differentiate between flyash and flyash-limestone mixtures by straight path transmission measurement based upon the data obtained during the laboratory tests.

### Scattering Measurements

Light intensity measurements as a function of the scattering angle  $\theta$  were made for different concentrations of both flyash and flyash-limestone mixtures. Of particular interest was the 90 degree scattering condition. These data are plotted in Figure 6. The measure of concentration is the same as that described for Figure 5. As with the transmission data, it is apparent that the presence of limestone has virtually no effect on side (90 degree) scatter intensity. Indeed, there is less than a factor of two difference between the mechanically and electrostatically precipitated dust samples.

The data of Figures 5 and 6 are cross-plotted in Figure 7, where straight path transmission versus 90 degree scattering curves are presented for mechanically and electrostatically precipitated flyash both with and without limestone. The slope of each curve at the origin is proportional to the scattering efficiency or  $\beta f(90^\circ)$  term in equation (6). These values are tabulated on the next page. It can be seen that the presence of limestone in the flyash has a minimal affect on the scattering efficiency of the dust. There is less than a factor of two difference in the spread of values measured, and no consistent trend.

The polar plots in Figures 8 through 10 were obtained using the scattering cell apparatus described previously. They show the angular variation in scattering intensity for electrostatically precipitated flyash both with and without limestone, and for mechanically trapped flyash without limestone. On each plot there are two curves. The right-hand curve is the apparent scattering from a beam. The left-hand curve represents single particle scattering, and is derived from the other

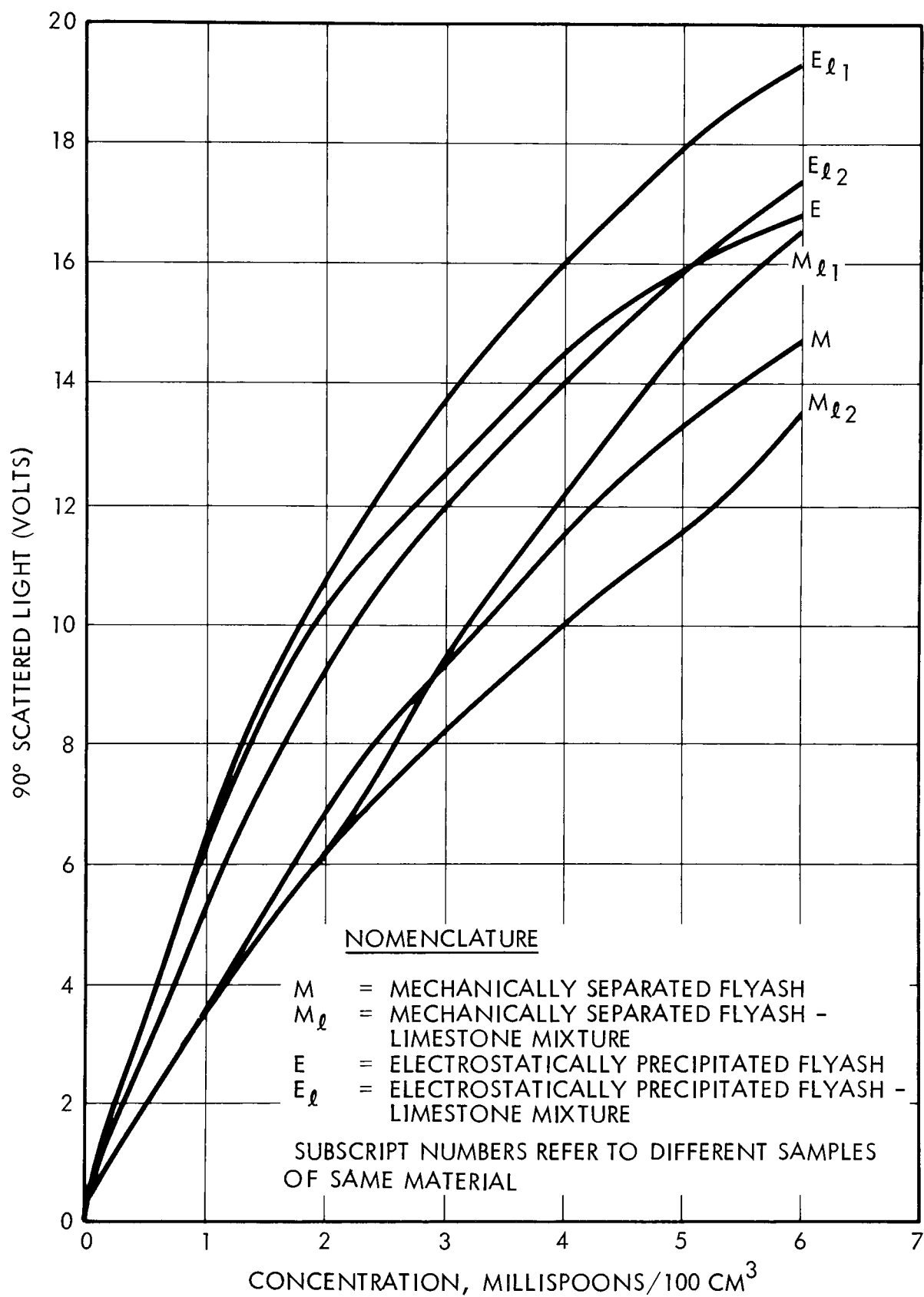


Figure 6. Ninety degree scattering of He-Ne gas laser light beam as a function of concentration for Unit 10 flyash and flyash-limestone mixtures.

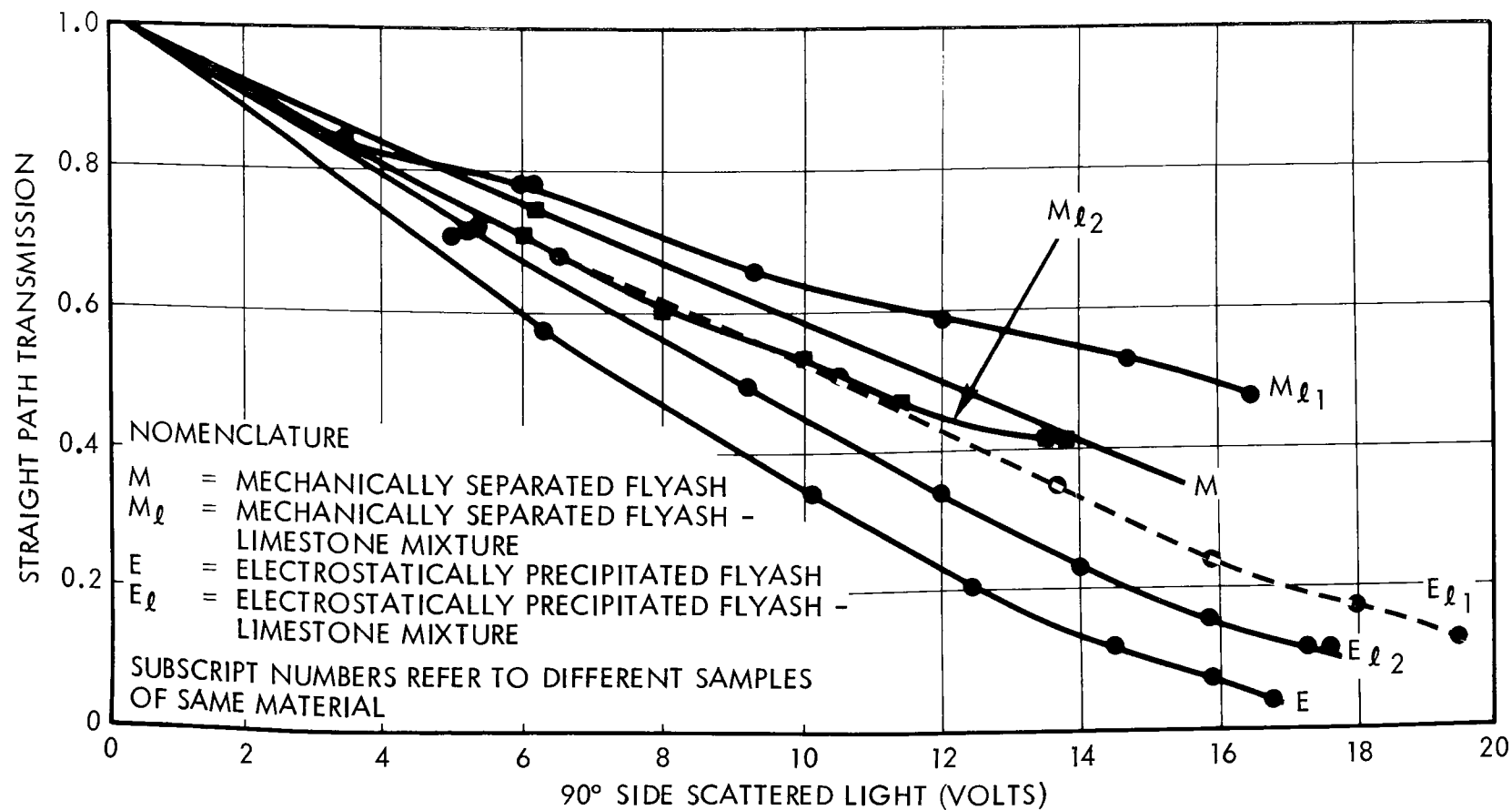


Figure 7. Straight path transmission versus 90° scattered light intensity for mechanically and electrostatically precipitated flyash samples with and without limestone.

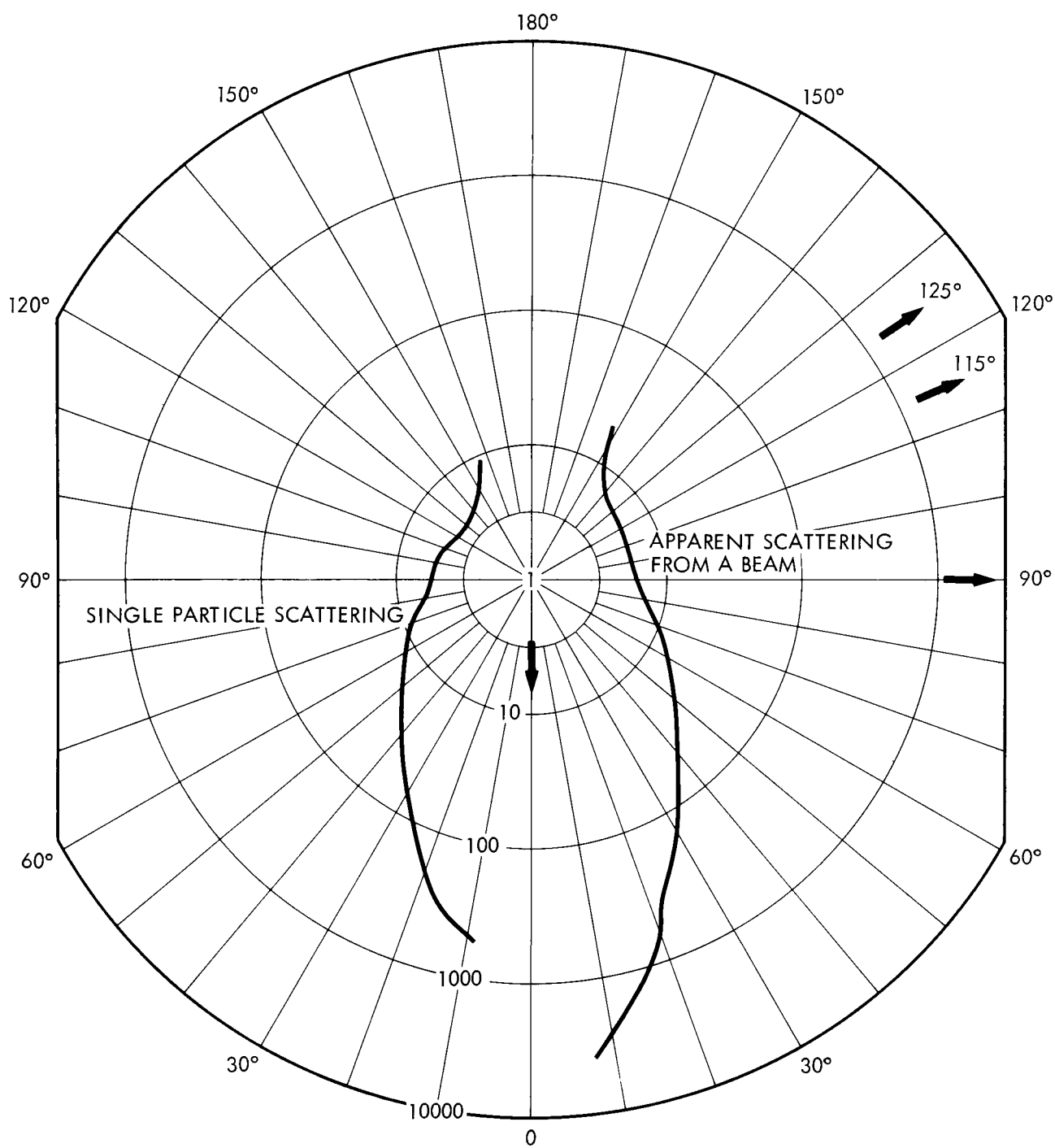


Figure 8. Polar plot of scattering intensity distribution for Unit 10 electrostatically precipitated flyash-limestone mixture.

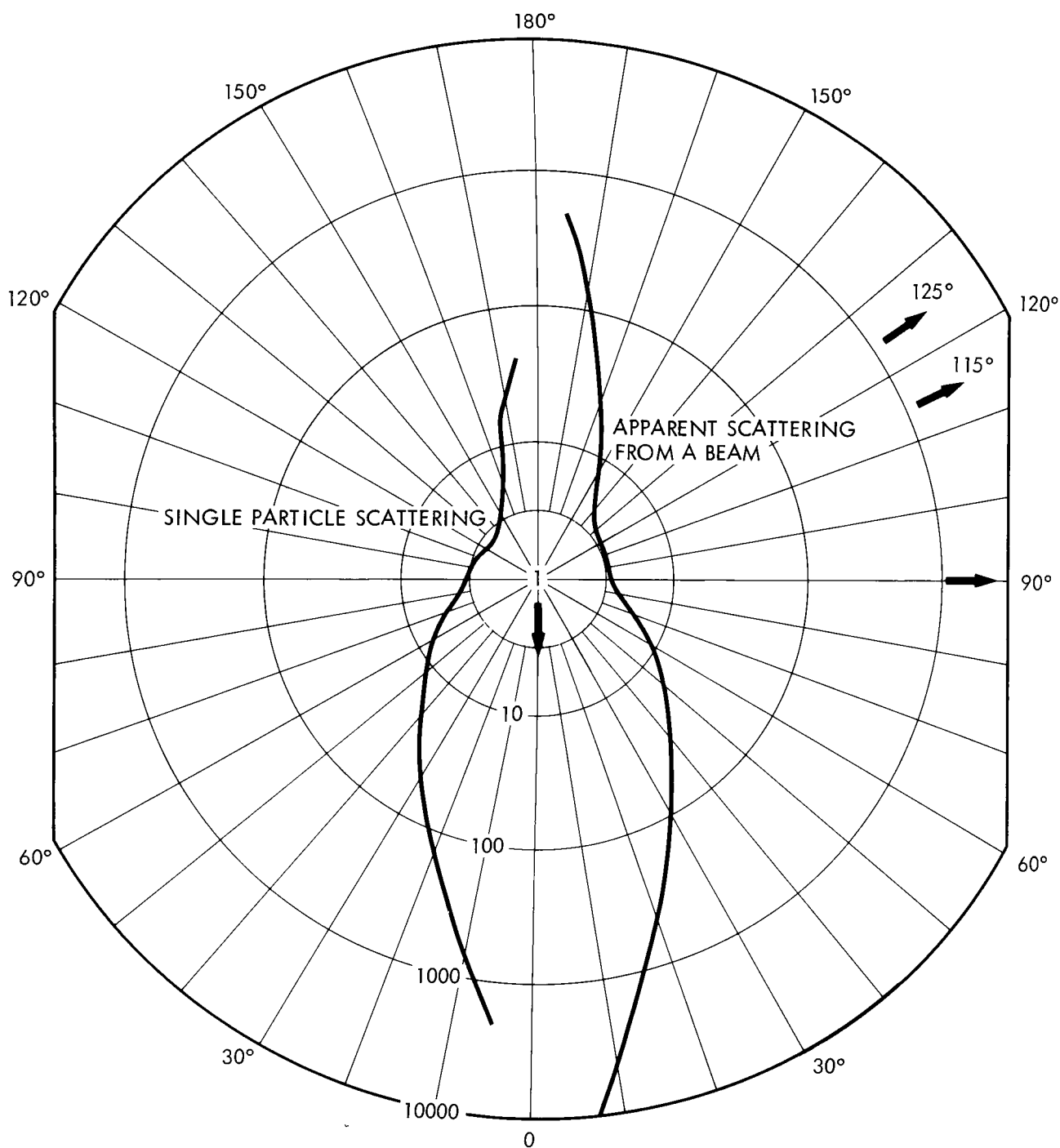


Figure 9. Polar plot of scattering intensity distribution for Unit 10 electrostatically precipitated flyash dust.



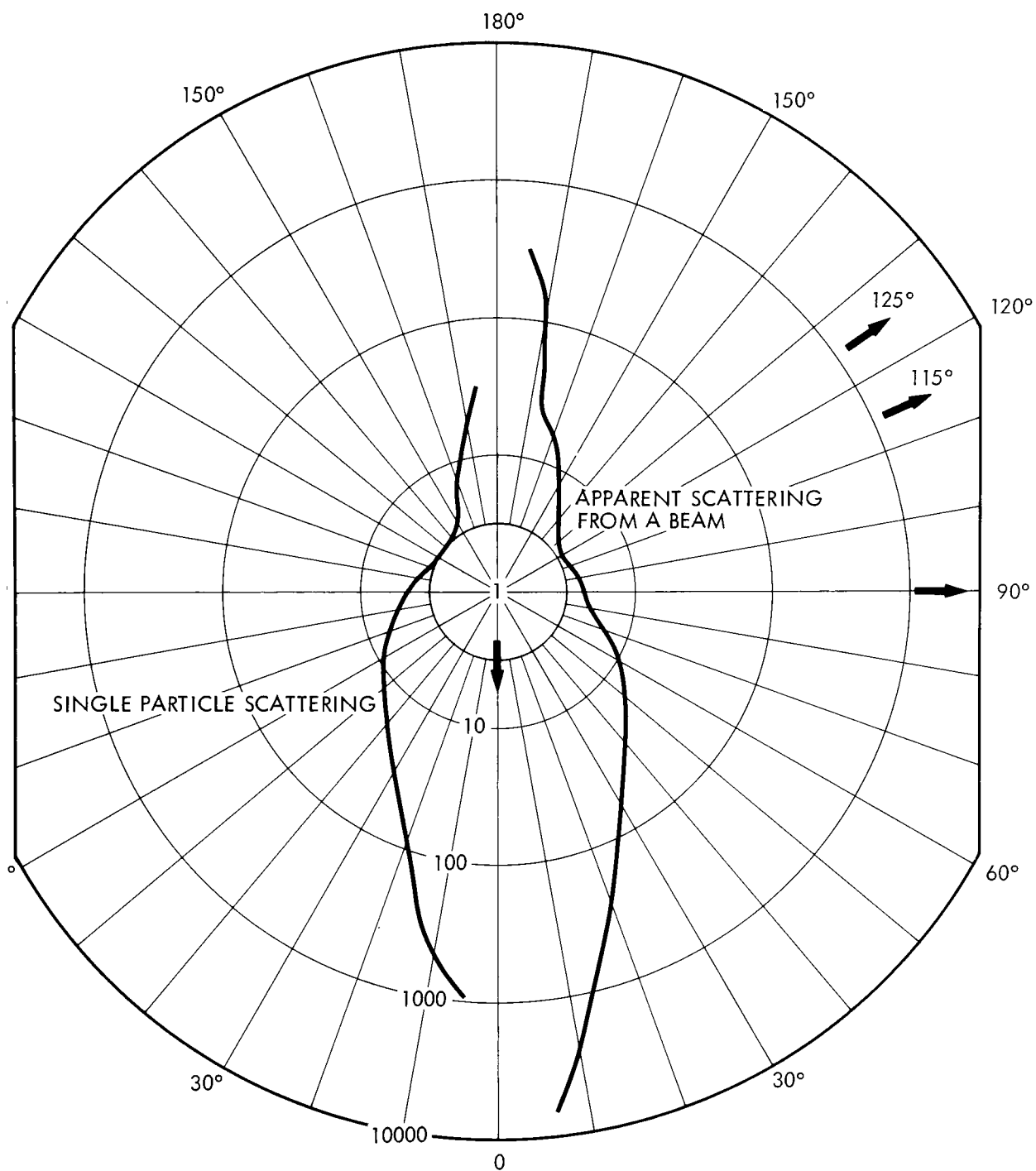


Figure 10. Polar plot of scattering intensity distribution for Unit 10 mechanically collected flyash dust.

Type	$\beta$ f(90°) Value
ESP flyash w/o limestone	.087
ESP flyash w/ limestone, #1 sample	.104
ESP flyash w/ limestone, #2 sample	.121
Mech. flyash w/o limestone	.138
Mech. flyash w/ limestone, #1 sample	.121
Mech. flyash w/ limestone, #2 sample	.12
Notes: ESP = Electrostatically precipitated flyash MECH = Mechanically separated flyash	

curve as follows: The intensity measurements of the laser beam scatter vary as beam intersection volume changes with the angle of measurement; i.e., the scattering volume =  $1/\sin \theta$  x constant, where  $\theta$  is the angle between the probing laser beam and the beam of scattered light received by the observing telescope (see Figure 1). When  $\theta = 0$  degrees (straight path transmission), the scattering volume is infinite. The observed scattering volume is a minimum value at  $\theta = 90$  degrees. To obtain single particle scattering, it is necessary to remove the geometric factor from the measurements by applying a  $\sin \theta$  factor. This results in the left-hand curve on each of the three polar plots. The data are normalized to transmission measurements as a function of particle concentration and thus all curves may be directly compared in the three plots. The curves are open at both the forward and back scatter ( $\theta = 0$  degrees and 180 degrees) regions due to limitations of the measuring apparatus setup.

An evaluation of these curves shows that only two significant scattering lobes exist with the predominant lobe in the direction of forward scatter ( $\theta = 0$  degrees). The scattering intensity is near a minimum at 90 degrees. The intensity of the forward scatter is estimated to be between 50 and 100 times greater than for the back scatter condition. In the scattering tests performed at the Shawnee Unit 10 boiler (described subsequently in Section 4.2), measurements were made at values of  $\theta = 90$ , 115 and 125 degrees. It can be seen from the polar plots in Figures 8 through 10 that the scattering intensities are minimal in this region.

A comparison of the polar plots of Figures 8 and 9, scattering intensity for flyash only and flyash with limestone, shows that there is little difference in the shape of the two curves or in the absolute values at any given angle. There is less than a factor of two difference in the scattering intensity between the two types of dust for values of  $\theta$  equal to those for which measurements were made at the Unit 10 boiler. This fact inhibits the detection or identification

of limestone dust in the presence of a background of flyash particulate. In short, the scattering characteristics of the two different types of dust proved to be remarkably similar.

### 2.3 PARTICLE MICROSCOPY

Determination of scattering characteristics of flyash by TRW Systems led to the discovery that some larger spherical particles in the samples were hollow and apparently filled with numerous smaller particles. This was revealed during a series of scanning electron microscope studies of flyash samples from the electrostatic precipitator and mechanical separator of the Unit 10 boiler. The work was a continuation of microscopy studies reported in Reference 2.

One of the first examples of a scanning electron micrograph which suggested that large hollow spheres contained smaller particles is seen in Figure 11. This is a ~1000X photomicrograph of a mixture of limestone and flyash obtained from mechanical separator hoppers of Unit 10. The arrow in the upper right-hand part of the photograph shows a ~30 micron sphere with a portion of its outer surface broken. It appears that smaller particles rest inside this shell.

Interest in this broken flyash particle resulted in a search for other such examples. To obtain some degree of particle separation, acetone was used to float the dust onto a pedestal before examination. Greater dispersion was achieved thus aiding the examination of individual particles. A second particle with a fractured shell was located and photographed using the scanning electron microscope. Three micrographs of one particle made at successively larger magnifications (~300X, 1000X and 3000X) are shown in Figures 12 through 14. Figure 12 is an overall view of the sample area scanned with the electron microscope. The particle of interest is ~80 microns in diameter. Surface details of the fracture and the internal ensemble of particles are more clearly seen in Figure 13. A more extreme enlargement (~3000X) of this particle is shown in Figure 14 where two distinct types of internal particles are clearly observed; namely, spherical and irregularly shaped particles in the two to 20 micron size range. The physical appearance of the two different types suggests that the spheres are probably smaller flyash particles resulting from the combustion of pulverized coal in Unit 10. The angular particles which look like "rock candy" strongly resemble photomicrographs of limestone calcined at ~1200°C as reported by McClellan in Reference 4.

Review of these rather dramatic photomicrographs raised the question of whether small particulate inside the larger flyash shell entered after the shell surface was fractured, or had somehow been encapsulated during the combustion process. In an attempt to answer this question, additional micrographic studies were made. The first two tests utilized the TRW scanning electron microscope. A small sample of dust from the Unit 10 mechanical separator was examined and then rolled with a metal rod to fracture larger particles. A photomicrograph of a deliberately fractured particle is shown in Figure 15. The results were considered indicative of

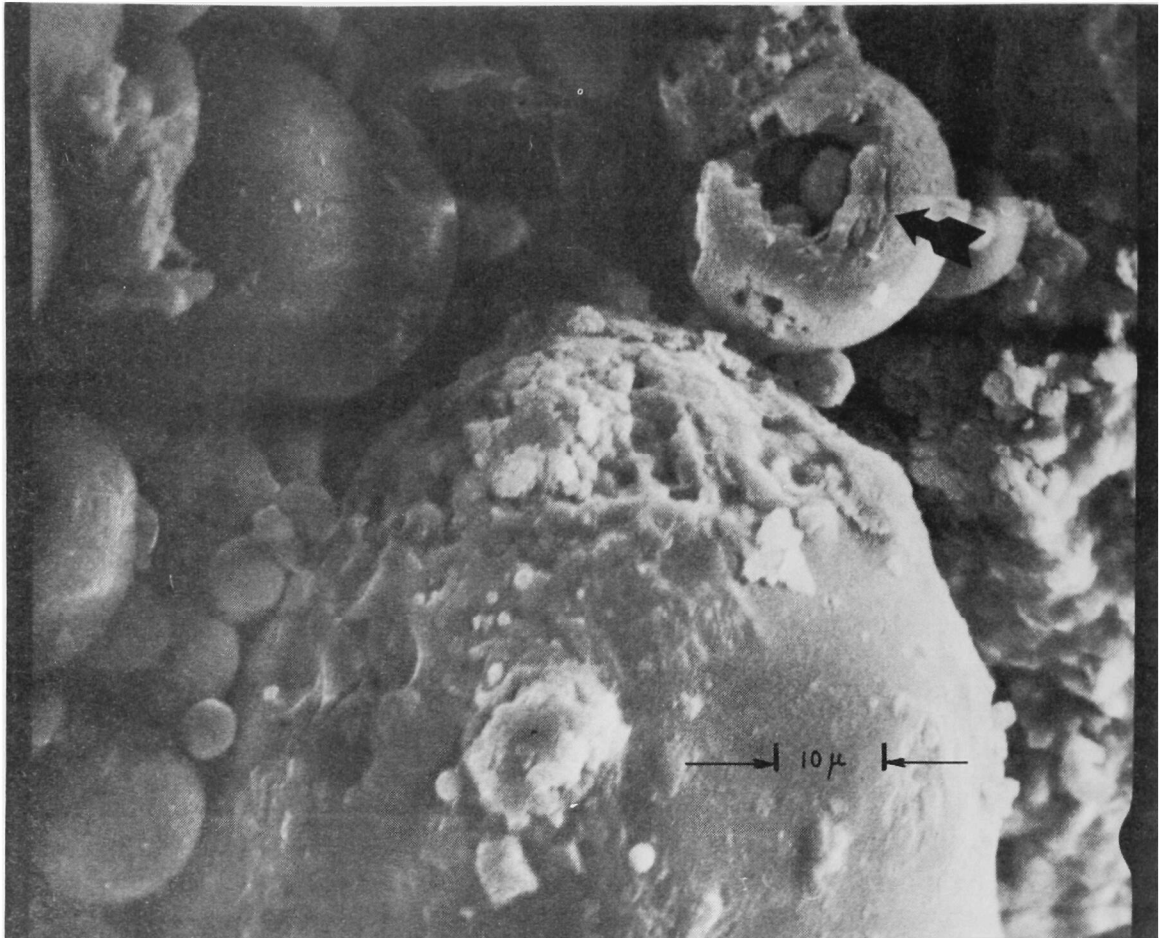


Figure 11. Scanning electron microscope (SEM) photograph of a fly-ash-limestone mixture in which a broken spherical particle (arrow) was observed to contain still smaller particles on the inside. The flyash sample was obtained from the hoppers of the mechanical separator on the Shawnee Unit 10 coal-fired steam boiler. Limestone dust was being injected into the furnace to remove SO<sub>x</sub> from the flue gases at the time this sample was obtained. Micrographs in all succeeding illustrations were made from Unit 10 flyash-limestone mixtures.

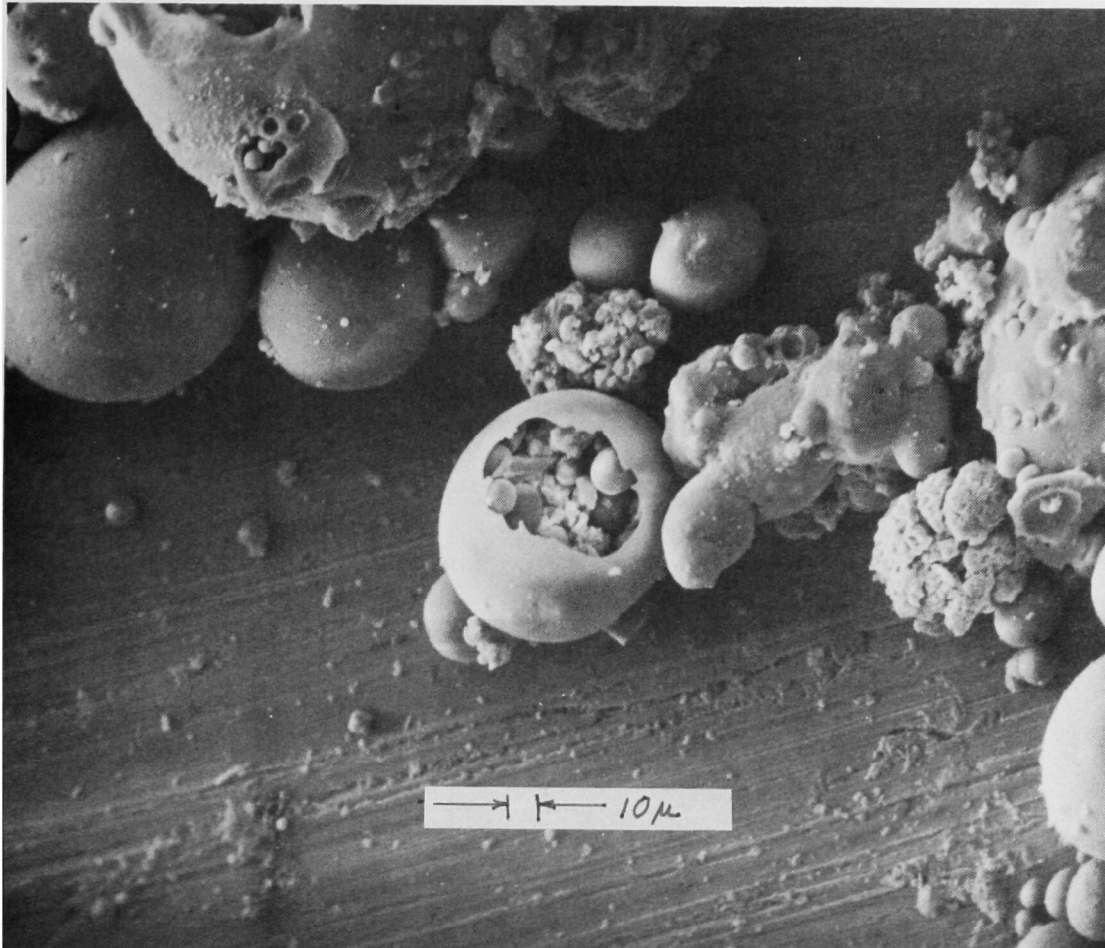


Figure 12. SEM micrograph (~300X) of broken flyash sphere showing internal particles. This micrograph was made in a deliberate attempt to find large broken particles containing smaller dust on the inside. Acetone was used to "float" the dust sample onto the SEM pedestal to achieve a greater degree of particle separation. The next two figures are photographs of the same broken particle but taken at magnifications of 1000X and 3000X, respectively.

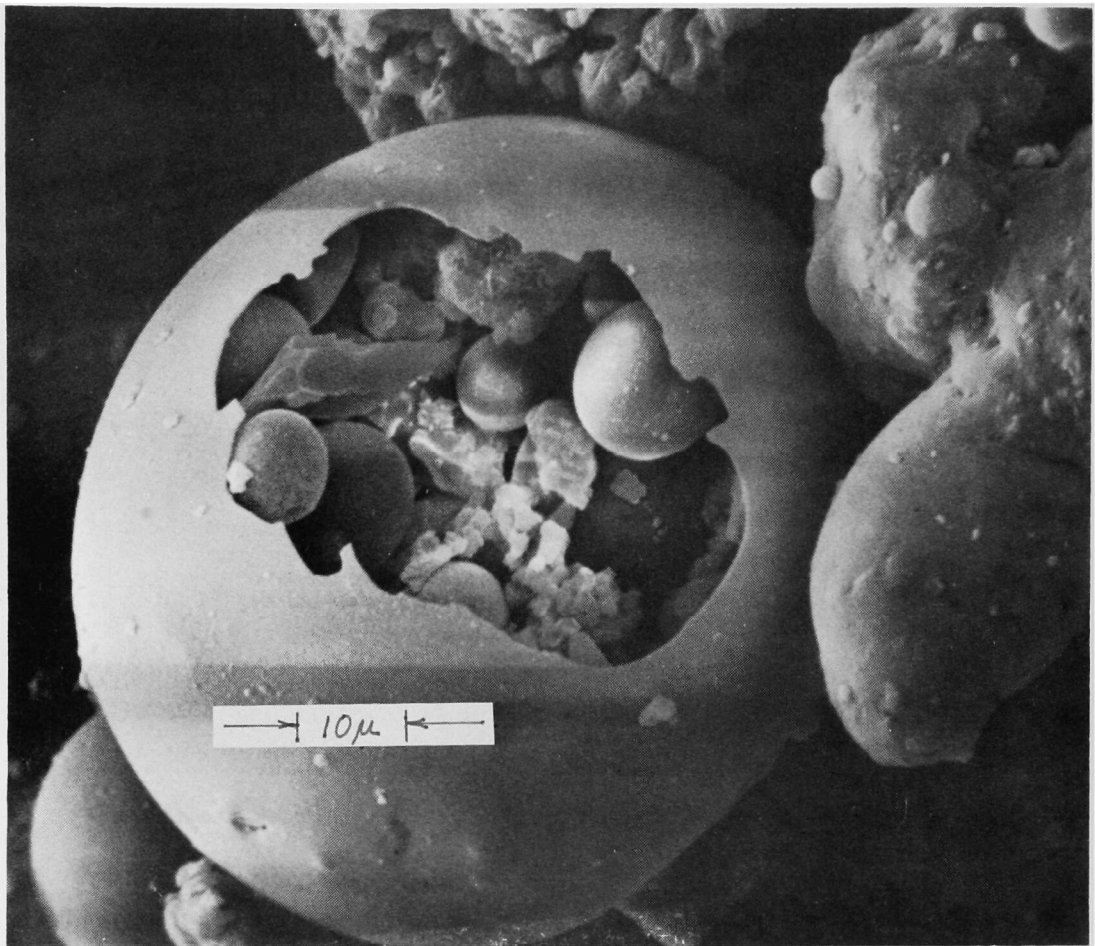


Figure 13. Higher magnification SEM micrograph of broken particle seen in Figure 12. This illustration clearly shows the contents of this hollow flyash sphere. Note the exceedingly thin wall of the hollow sphere. Particle diameter is about 80 microns. When this micrograph was made, it was not known if the internal particles had fallen in after the shell was broken or had been encapsulated during the combustion process.

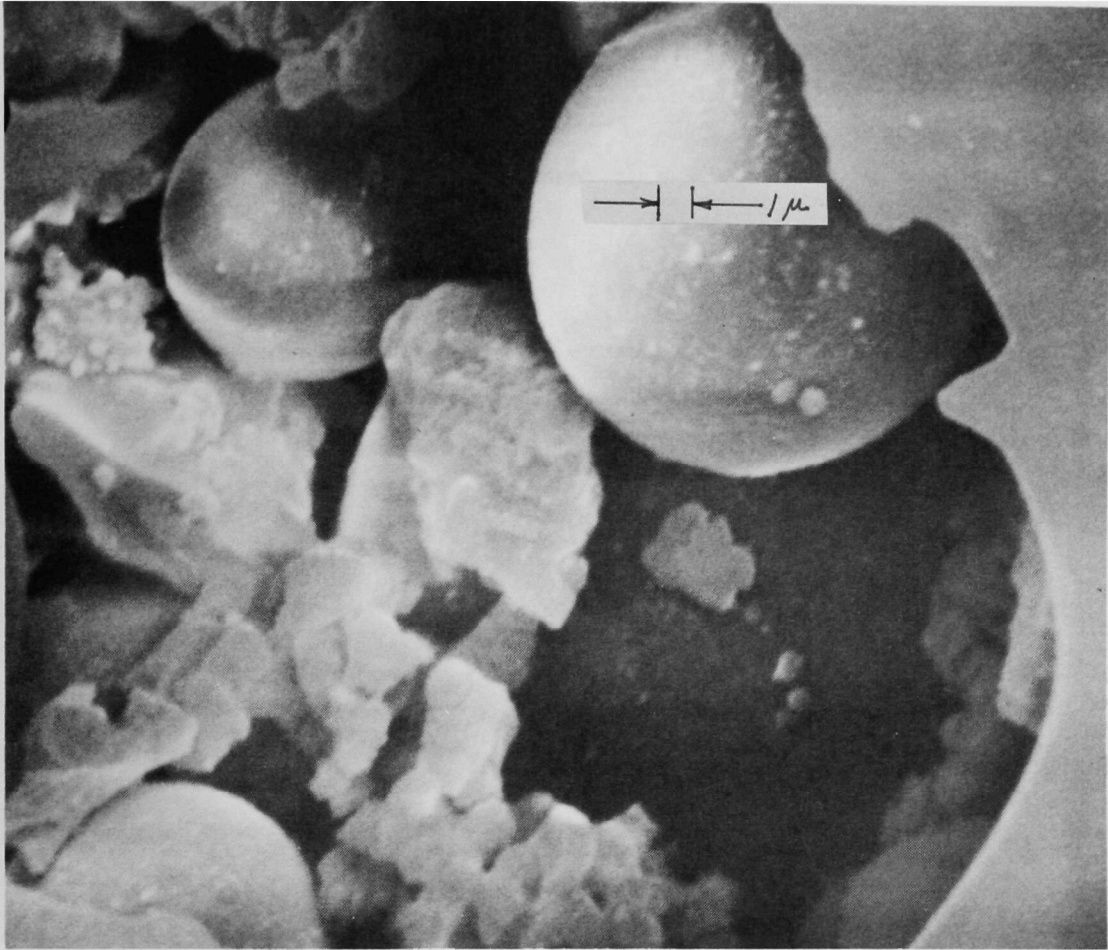


Figure 14. Extreme enlargement of Figure 12 showing contents of hollow flyash sphere. Note the two distinct types of particles. The spherical particles are thought to be small flyash dust while the angular "rock candy" particles are believed to be calcined limestone. Microprobe analysis is needed to identify the particle chemistry.



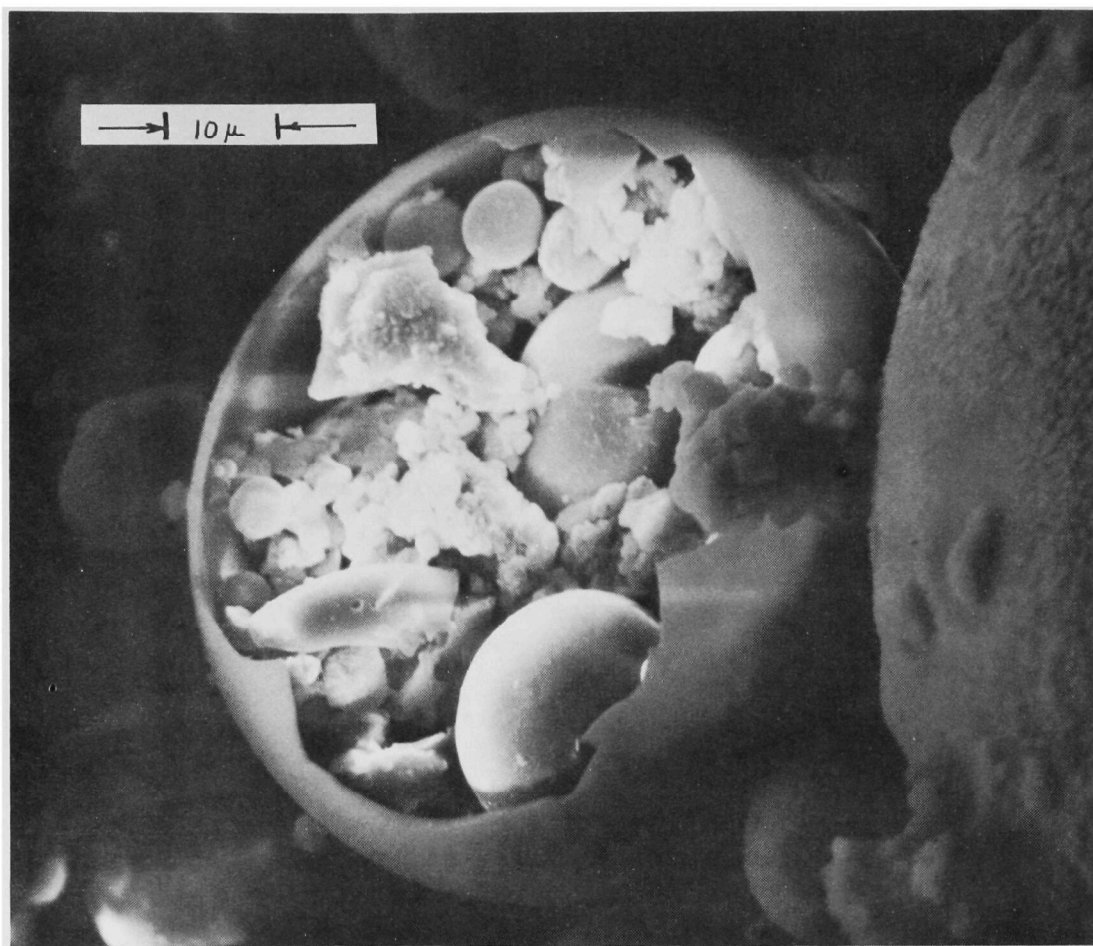


Figure 15. SEM micrograph of flyash particle broken by rolling a metal bar over a dust sample. This was an early attempt to determine if the smaller particles were originally encapsulated in the larger sphere or had fallen into the void after the shell was broken. Although indicative that the internal dust was trapped during the combustion process, this test did not fully confirm the fact.



an encapsulation process; however, the micrograph could not be considered as conclusive evidence since the rolling method of fracture could also have introduced smaller particulate into the hollow sphere.

Another and more unique method was tried. The micrographs of Figures 16 and 17 show the results of the new method. In each instance, a large unbroken flyash particle was located in the field of view of the scanning electron microscope. The electron beam was concentrated at the surface of the flyash particle. Localization of the beam energy caused the surface material to melt away. Evidence of the molten state of the flyash shell is easily seen in the two figures. The porous nature of the surface in the region of the molten particle wall suggests that outgassing occurred during the melting process.

In Figure 16, the opening in the flyash particle is approximately 45 microns maximum width. The opening in the companion micrograph is about 80 microns. In each instance, the internal volume of the flyash sphere is full of smaller particles. All examples in the preceding illustrations were taken from flyash-limestone mixtures obtained from Unit 10 at Shawnee. The encapsulated particulate in all cases seemed to consist of both smaller flyash spheres and the irregularly shaped glossy particles thought to be calcined limestone.

In addition to the scanning electron microscopy studies under the present contract (CPA 70-4), further microscopic studies were done under TRW sponsorship using a conventional light microscope. Flyash is typically a fused silicious residue with a glassy transparent appearance.<sup>5</sup> This allows one to conveniently observe particle structure and characteristics using transmitted light and a high quality light microscope. The following micrographs were made in this manner using an Izumi Polarization Microscope (S/N 19637) with a Polaroid film back adaptor and various objective lenses.

Selected particles from samples of Shawnee Unit 10 flyash (mechanical collector) were crushed while under observation so that the fragmentation process could be observed. A small quantity of dust was scattered on a microscope slide. From this ensemble, a single particle of spherical shape and white color was removed with the aid of a 12X eye loupe and a teasing wire. The selected particle was then immersed in a drop of dioctyl phthalate (DOP) oil on another microscope slide, and covered with two 0.020 inch thick cover glasses. The thickness of the double cover glasses very nearly matched the distance between the particle and the barrel of the microscope objective lens at its focal distance. It was possible, therefore, to use the microscope focusing mechanism to apply pressure to the particle with the lens barrel while the particle was under observation.

Micrographs of individual particles were recorded. The microscope objective lens was then depressed until the particle was observed to fracture. Further disintegration was observed as additional force was exerted. Micrographs were recorded at various stages of this process.

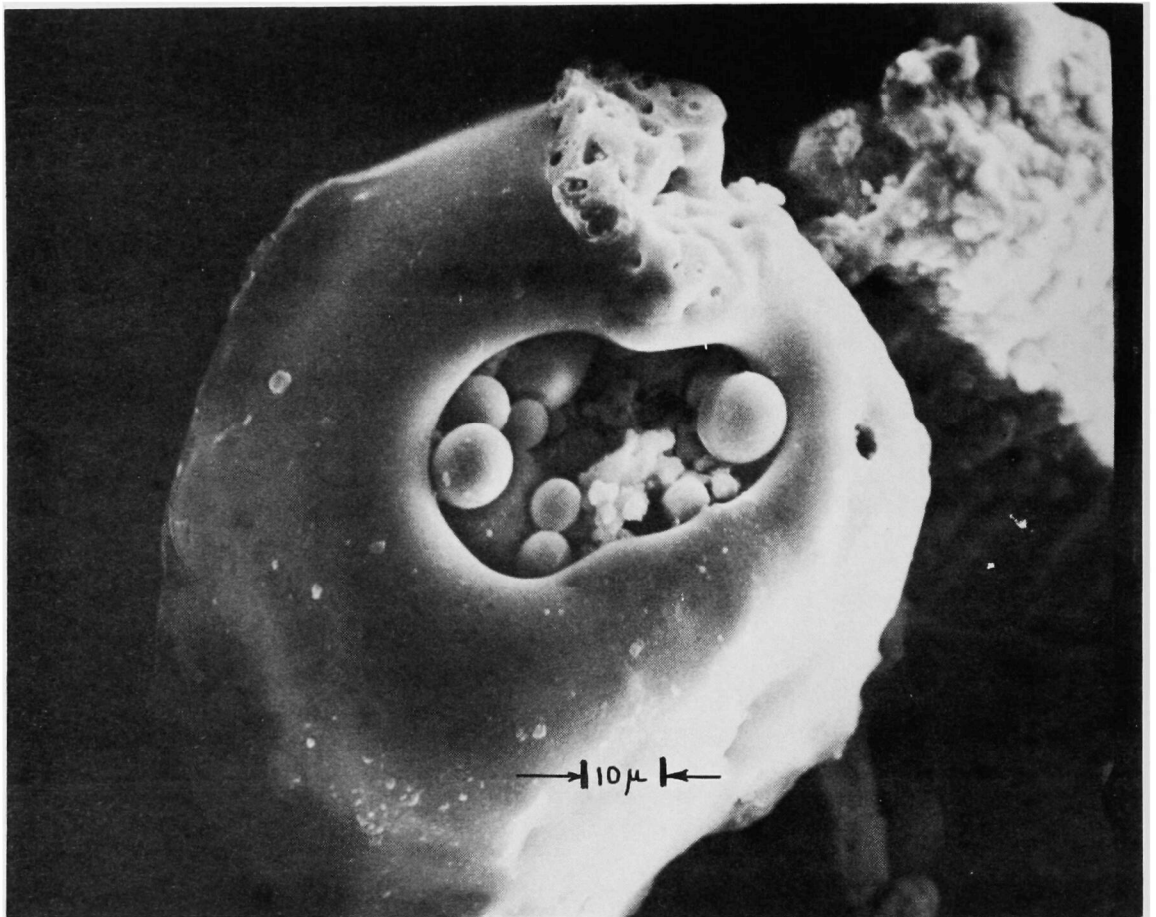


Figure 16. SEM micrograph of flyash particle with hole melted in previously unbroken surface by concentrating the energy of the electron beam at the surface. This and subsequent micrograph using this technique revealed numerous small particles inside the large particle thus tending to confirm that encapsulation occurred during combustion process.

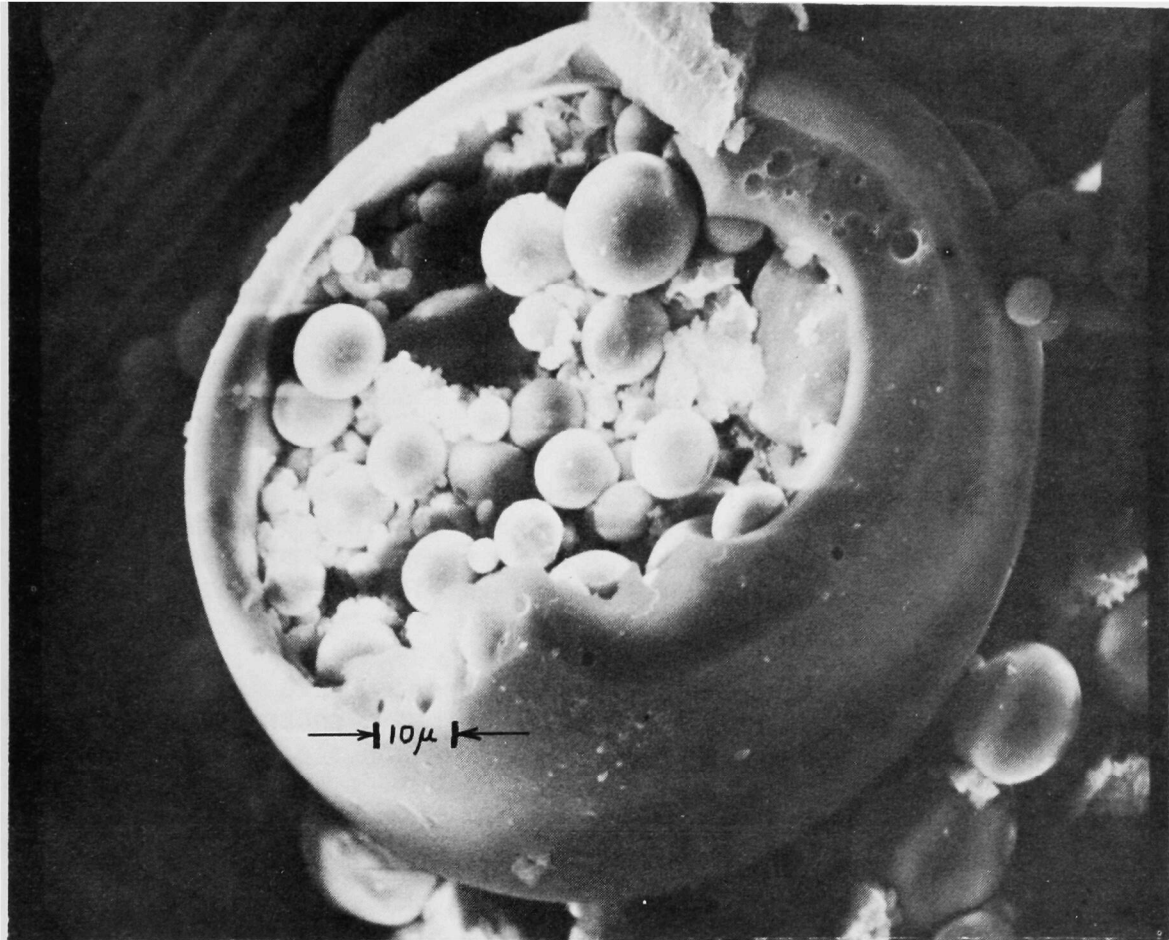


Figure17. SEM micrograph of a second flyash particle in which the surface was melted using the concentrated energy of the electron beam. Note the voids in the edge of the encapsulating shell suggesting that entrapped or dissolved gases were liberated as the result of the material being heated by the electron beam.

The two 400X micrographs of Figure 18 illustrate an 80 micron diameter spherical flyash particle photographed before and after fracture. The upper photograph shows the particle intact and clearly demonstrates that smaller particles are encapsulated in this larger sphere. The other photograph was made after the particle had been broken by the method described. A portion of the larger particle has drifted to the left. The pieces of this particle are still immersed in the oil film between the two glass slides which serves to hold the fragments within the field of view.

The series of six micrographs in Figure 19 show several progressive stages of particle disintegration (from left to right) as a result of repeatedly squeezing the entrapped large particle. In its original form, the flyash particle was approximately 150 microns in diameter (Figure 19a). Definite major fracture lines are seen in Figure 19b. The existence of one interesting 15 micron particle is followed (arrow) in each of the micrographs. In the last micrograph (19f) this smaller particle had also been fractured.

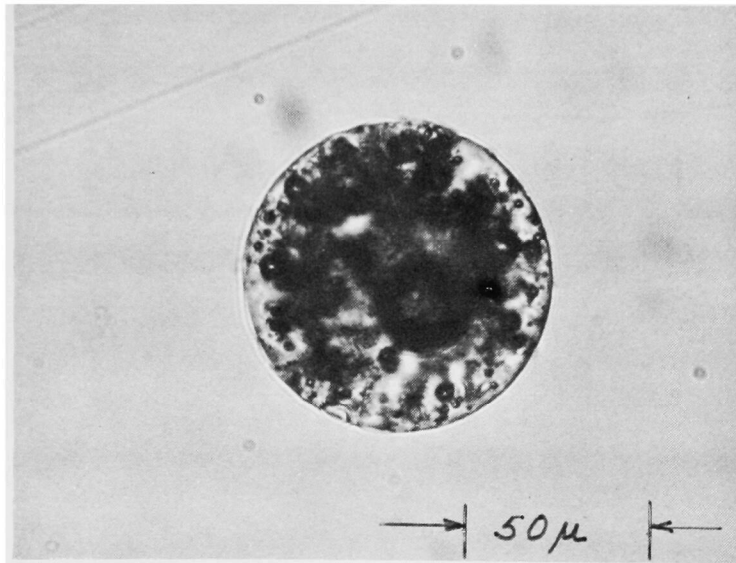
The last illustration (Figure 20) is a lower power (160X) micrograph of a small particle (arrow) partially assimilated into a larger 140 micron diameter particle. The smaller particle is perhaps 50 microns in diameter. Several particles of ~10 microns diameter are also seen attached around the outside of the large particle.\*

As mentioned, the particle microscopy reported here is a continuation of work begun under an earlier portion of the basic contract and reported in Reference 2. The microscopy was initiated as an aid to understanding the scattering characteristics of the Unit 10 flyash and limestone-flyash mixtures. In the process of examining various samples of ash, the containment of very small particles by larger spheres was noted and investigated. This work continued to a point where it could be confirmed that the small particles were indeed encapsulated during the combustion process and did not, as first suspected, become entrapped in the cavities of previously broken large spheres.

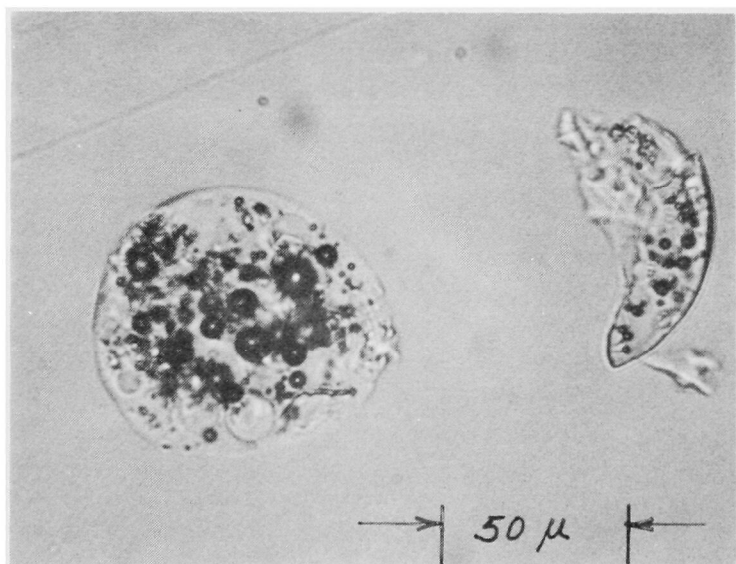
It is suggested that the encapsulating phenomena is important from two considerations. If a mechanism by which the encapsulation takes place can be understood, it may be possible to enhance or promote the process thus reducing the number of fines in the stack gas. Conversely, if particle collection methods tend to fracture the thin shells of larger spheres, the possibility exists that additional microscopic dust may be introduced into the stack gases. The investigation of flyash formation and encapsulation processes was not within the scope of the present work; however, additional work and understanding in this area would seem quite worth while.

---

\* The dark curving line in the upper portion of this micrograph is the edge of the DOP oil droplet in which the flyash particle was immersed.

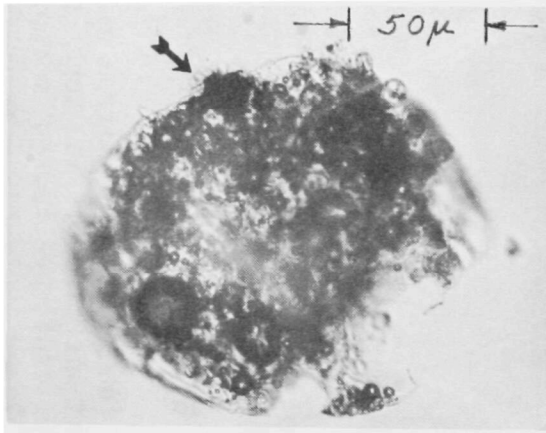


(a)

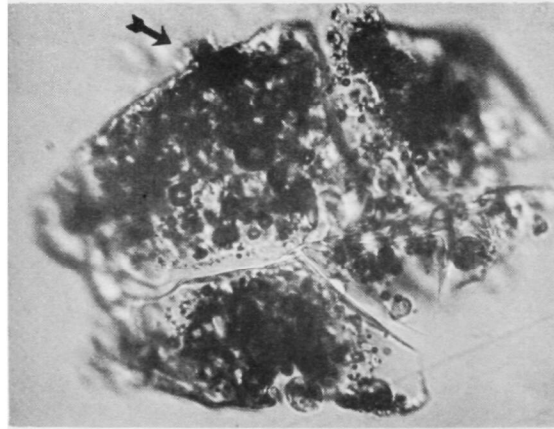


(b)

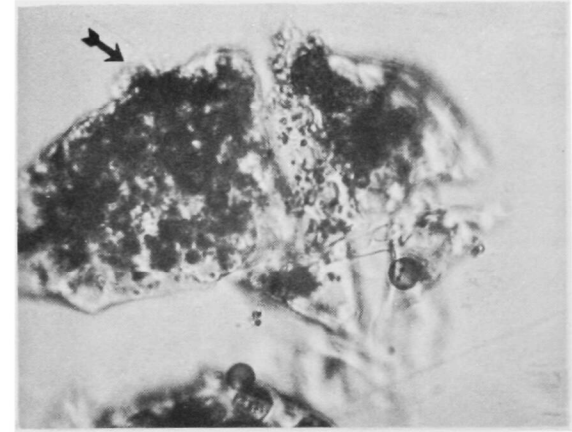
Figure 18. Transmission micrographs (400X) of an 80 micron diameter particle made with a light microscope. The upper photograph clearly shows the internal particulate encapsulated in a flyash sphere. The lower photograph was taken after the sphere was broken.



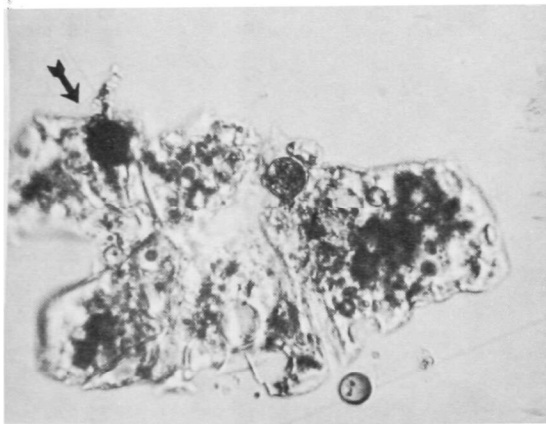
a



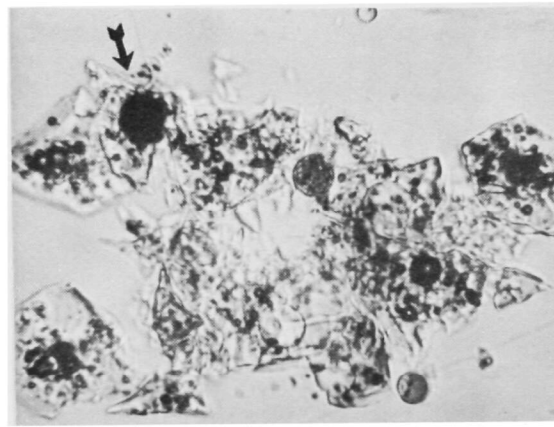
b



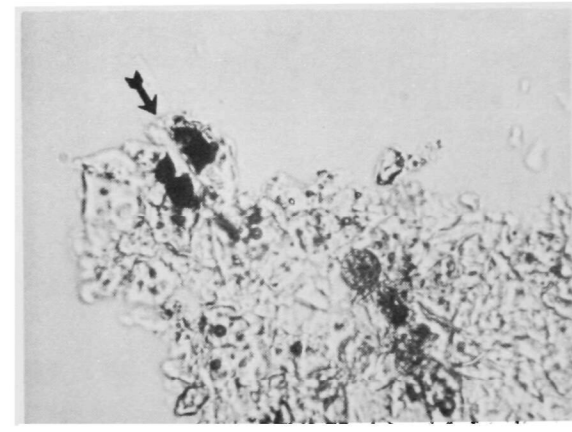
c



d



e



f

Figure 19. Six micrographs of a large 150 micron particle showing the progressive disintegration of the structure under increasing pressure from the light microscope objective lens. Several small internal particles can be traced in the disintegration process. Observation of particle breakup was continued until one of the internal particles (arrow) was eventually broken. At this point, most of the residue was  $\leq 10$  microns.

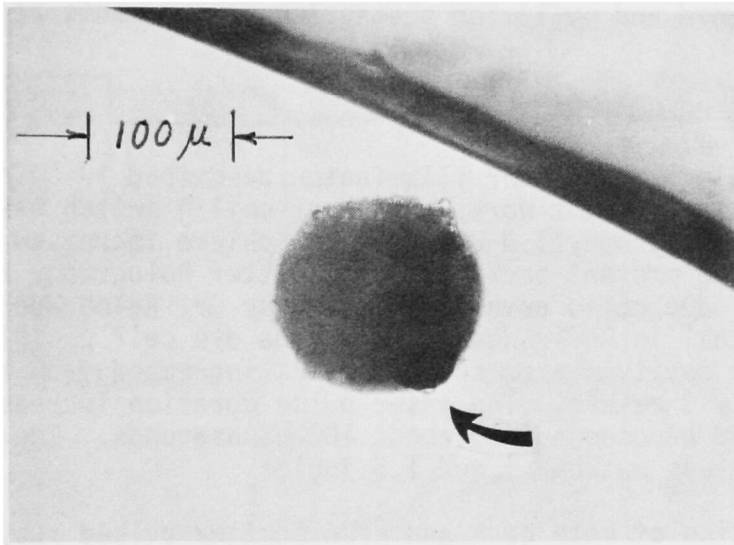


Figure 20. Micrograph (160X) of a small 50 micron particle partially imbedded in a larger 140 micron flyash particle.

### 3. EXPERIMENTAL EQUIPMENT

The apparatus used during the experimental effort on this program is conveniently divided into two categories. The first concerns the holographic tests conducted in a TRW Systems laboratory, while the second consists of equipment designed and built for scattering measurements at the Shawnee Unit 10 boiler.

#### 3.1 RUBY LASER HOLOCAMERA

The TRW pulsed ruby laser illuminator described in Reference 2 was again used for the present work. The Kerr cell Q switch was removed and replaced with a Chlorophyll *d* dye cell to achieve increased laser coherence necessary for the present back and side scatter holography application. The Chlorophyll dye cell, developed at TRW by Dr. Ralph Wuerker, is reported in detail in Reference 6. With the dye cell positioned in the ruby oscillator cavity, laser coherence was increased from a few centimeters to approximately 3 meters. The laser pulse duration increased from approximately 50 nanoseconds to about 100 nanoseconds. Energy content of the laser pulse was between 1 and 1.5 joules.

Demonstration of both back and side scatter pulsed ruby laser holography necessitated construction of different holocamera configurations. All of the holography during the present work was accomplished in a large laboratory using breadboard configurations. The schematic diagram of Figure 21 shows the arrangement used for holographically recording ruby laser back scatter. The arrangement is a three beam system similar to that used in the earlier transmission holography.<sup>2</sup> The ruby laser output beam is divided into two components using a wedge beam splitter. Approximately 90 percent of the ruby light passes through the beam splitter (W-1) to form the scene beam. A right angle prism diverts the incident scene beam into the scattering medium of the scene. A reflection off the first surface of the scene beam prism is incident on a photodiode used to monitor the ruby laser output. That portion of the ruby laser light reflected by the wedge beam splitter is expanded and collimated into a 5-inch diameter reference beam using a telescope. The collimated light of the reference beam is further divided into two beams with the aid of a second wedge (W-2). Reflected light from the second wedge beam splitter is directed onto the hologram using a front surface mirror (M-1). A second front surface mirror (M-2) reflects the remaining reference illumination transmitted through the second beam splitter (W-2) onto the hologram. The path lengths of the two reference beams are matched.

The hologram is located adjacent to the scene beam such that low angle (<5 degrees) back scatter may be recorded. In tests made to date, back scatter of pulsed ruby laser light over distances of up to 15 feet have been successfully recorded. Test aerosols have included chalk dust and dioctyl phthalate (DOP). These tests were essentially the same as earlier work<sup>2</sup> except that a second reference beam was added as in the previous transmission scattered light holograms.



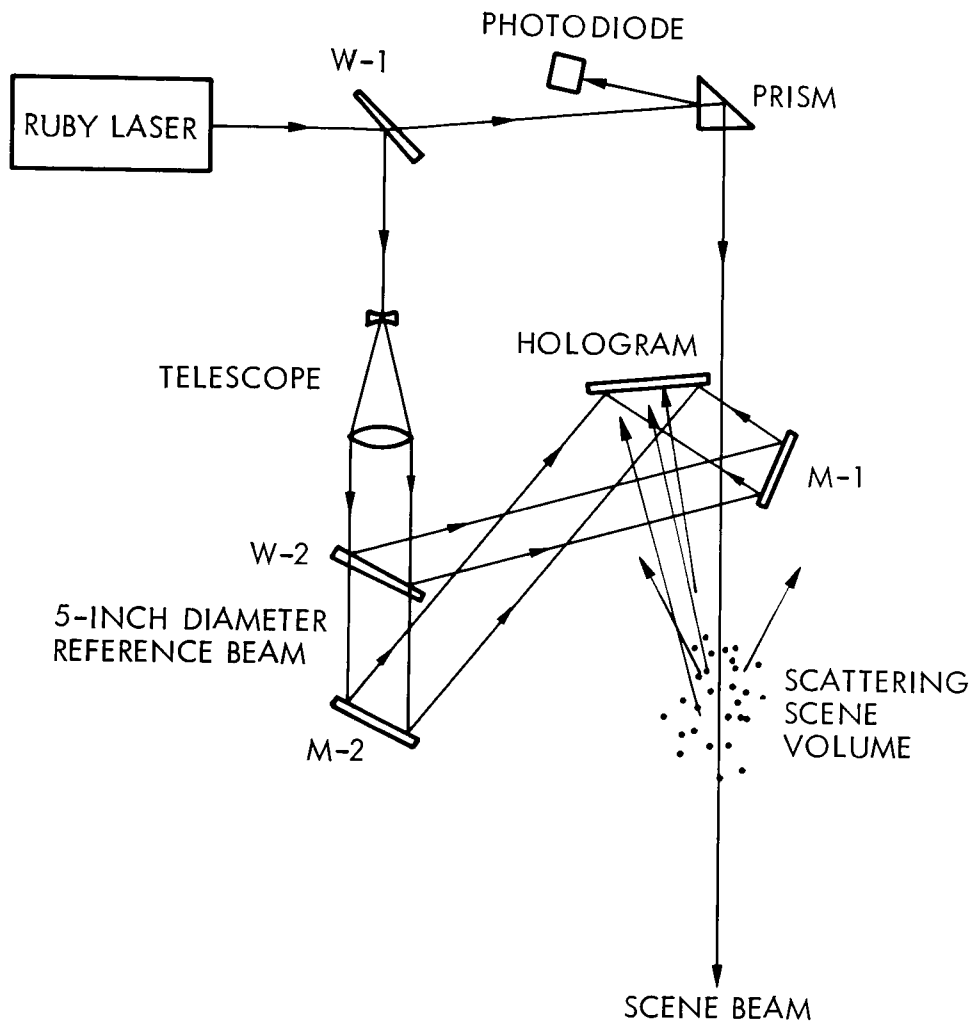


Figure 21. Schematic diagram of laboratory holographic arrangement used to record back scatter of a ruby laser scene beam.

Port geometry and availability at elevation 376 at Shawnee Unit 10 suggested an alternate holographic arrangement, namely the recording of side scattering of the incident scene beam. The holography of side scattering (90 degree scattering) offered a potential for covering more lateral area in the plane of interest at this boiler elevation.\* For this reason, the feasibility of recording side scatter of a pulsed ruby laser beam was investigated in the laboratory. A breadboard holocamera was setup to demonstrate feasibility of the technique. A schematic diagram of this holographic arrangement is shown in Figure 22. For the sake of simplicity, the second reference beam was omitted in this setup. A two beam holocamera was adequate for demonstrating the feasibility of holographically recording side scatter from the ruby laser scene beam.

From Figure 22, it will be seen that the output of the ruby laser was divided into scene and reference components using a wedge beam splitter (W-1). The reference beam was expanded and collimated into a 5-inch diameter beam using a telescope. Two front surface mirrors (M-1 and M-2) directed the reference beam onto the holographic plate. Light transmitted through the wedge beam splitter (W-1) formed the scene beam. Two 90 degree prisms (P-1 and P-2) were used to direct the scene beam in front of and parallel to the holographic plate. The distance between the scene beam and film plate was approximately 6 feet. For some tests, a cylinder lens was placed in the path of the laser beam reflected by prism P-2 to form a fan-shaped scene beam. With the configuration shown in Figure 22, a nominal scene width of 4.5 feet could be obtained establishing a viewing angle of about 37 degrees. When the cylinder lens was used, the maximum width of the fanned beam was about 1 foot. The scene width was 4.5 feet.

With the holographic arrangement described, both static scenes and aerosols were recorded. The purpose of these tests was to show the basic feasibility of holographically recording side scatter of a probing ruby laser scene beam. Holograms of static objects were first recorded and successfully reconstructed. Tenuous aerosols of chalk dust and DOP were subsequently recorded. Reconstructions of side scattering by aerosols were, in general, not as satisfying as similar recordings of forward and back scattering of a ruby laser beam. The side scatter holograms were not as bright. This result was not unexpected based upon the angular scattering intensity distribution measurements made earlier in the program (see Section 2.2). Quantitative measurements of the aerosol number density from variations in scattering intensity recorded by the hologram were not attempted during these feasibility experiments.

\*

A holocamera for recording side scattering at Unit 10 was designed during the course of the present work. It is presented and discussed in Section 4.

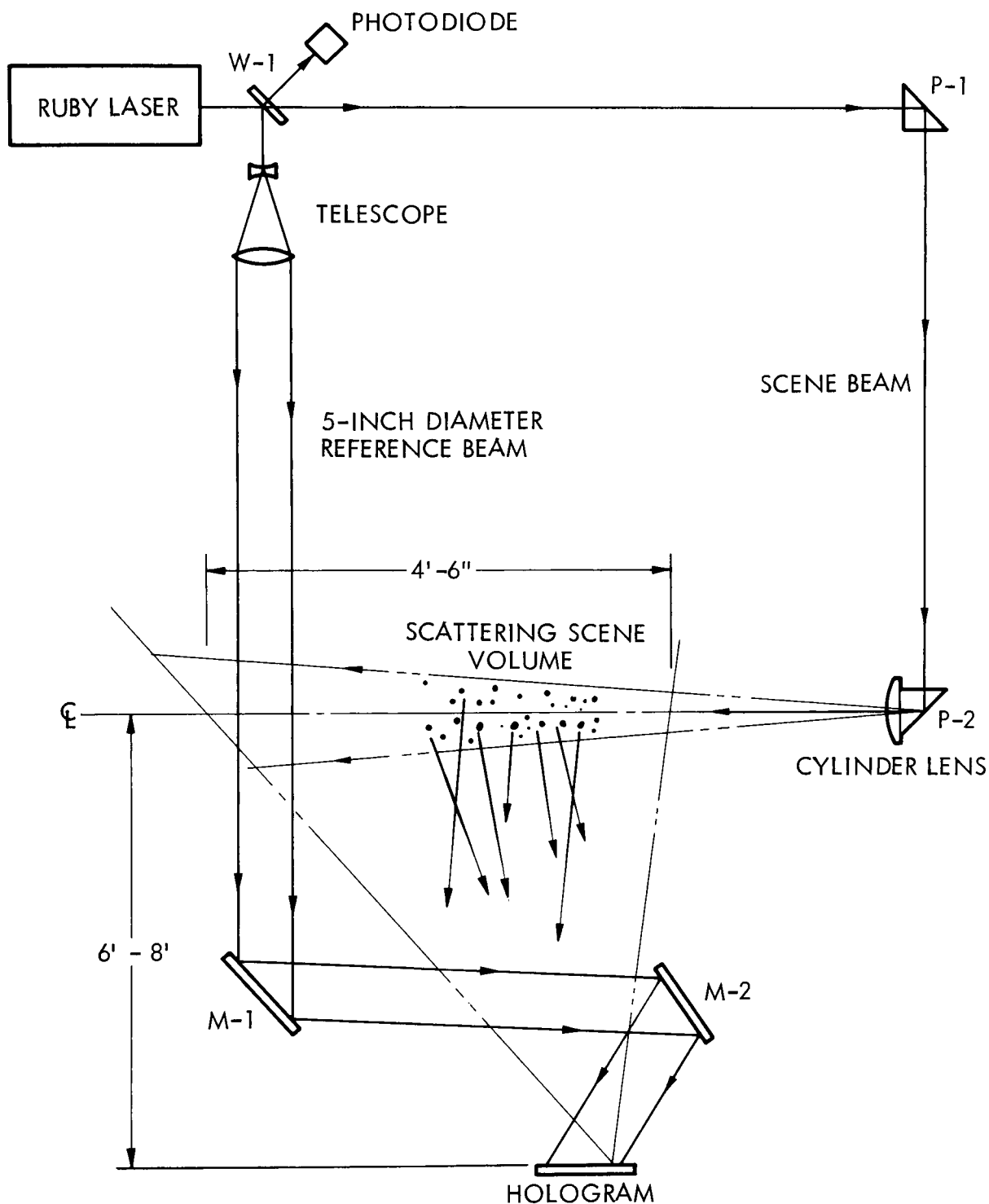


Figure 22. Schematic diagram of holographic arrangement used to record side scattering of ruby laser scene beam during laboratory feasibility tests.

### 3.2 SYNCHRONOUS DETECTOR

Although back and side scatter pulsed ruby laser holograms of tenuous aerosols could be made under laboratory conditions, the utilization of this technique at the Shawnee Unit 10 boiler remained to be determined. It was desired to study limestone particulate distributions in the presence of flyash, at elevation 376 of the boiler. A series of transmission measurements at this elevation under various boiler operating conditions would enable one to determine the potential and limits of the holographic technique at this elevation. Unfortunately, opposed ports did not exist at the 376 elevation and hence, no measure of the optical thickness of the scene volume could be easily obtained. As a result, it was decided to build and test a helium-neon gas laser illuminated synchronous detection system for measuring the power of the scattered laser light under various geometry and boiler operating conditions.

The diagram in Figure 23 shows schematically the components of the laser illuminated synchronous detection system which was constructed and tested at elevation 376 of the Shawnee Unit 10 boiler. The illuminator is a continuous wave Spectra Physics Model 124A helium-neon (He-Ne) gas laser which emits approximately 18 milliwatts of visible red light at a wavelength of 0.6328 micron. The light is collimated in a 1.1mm diameter beam. The d.c. light signal produced by the laser is converted to an a.c. output with the aid of a chopper. The light chopper consists of an 1800 rpm synchronous motor driving a 25 tooth gear which intersects the laser beam. The result is a 750 Hz square wave light signal. Light pulses passing between the gear teeth are directed into a scattering medium of interest (i.e., particulate in the boiler combustion gases). Laser light reflected by the gear teeth is incident on a photocell which generates a 750 Hz electrical reference signal for the lock-in amplifier (Figure 23).

Background flamelight in the boiler was sufficiently intense that light scattered from the 18 milliwatt probing laser beam by particulate entrained in the combustion gases could not be observed with the unaided eye. To make scattered light measurements, a very large improvement in signal-to-noise ratio was required. This was accomplished by several means. The principal improvement came through use of the synchronous detector system consisting of the light chopper and lock-in amplifier. The lock-in amplifier, an EMC, Inc. Model RJB, comprised a resonant signal amplifier, inverter, gating circuit and averaging circuit. The six db/octave time constant  $\tau$  of the averaging circuit defines both the rise time of the measurement and the equivalent bandwidth  $f = 1/(\pi\tau)$  of the system, centered at the reference frequency of 750 Hz. A reference frequency of 750 Hz was selected because this frequency is neither a harmonic of 60 Hz nor of 120 Hz and, therefore, should give good discrimination against these power-related noise frequencies.

The chopped laser beam scattering intensity is observed and measured using a focusing telescope and photomultiplier tube (PMT). The telescope and PMT assembly, mounted on a rotating azimuth head is shown in the

LIGHT CHOPPER  
(1800 RPM SYN. MOTOR  
WITH 25 TOOTH GEAR)

C-W He-Ne LASER

$.6328\mu$  AT 750 HZ

SCENE  
(SCATTERING)

SILICON LIGHT  
DETECTOR  
(REFERENCE SIGNAL  
GENERATOR)

POWER SUPPLY  
HARRISON 6515A  
0-1000 V

HEAT ABSORBING  
(I.R.) GLASS FILTER

NARROW BAND ( $.6328\mu$ )  
GLASS FILTER

1 MM<sup>2</sup> PINHOLE IN MIRROR FOR FOCUSING  
EYEPIECE OF TELESCOPE

PHOTOMULTIPLIER  
TUBE (1P21)

A.C. COMPONENT OF  
OPTICAL BACKGROUND  
NOISE

CA  
PLUG-IN  
PRE-AMP

TEKTRONIX  
535  
OSC.

EMC, INC. MOD. RJB  
LOCK-IN  
AMPLIFIER

COHERENT  
LIGHT  
SIGNAL

BRUSH TWO -  
CHANNEL  
CHART RECORDER

REF. SIGNAL INPUT

Figure 23. Schematic diagram of laser illuminated synchronous detection system.

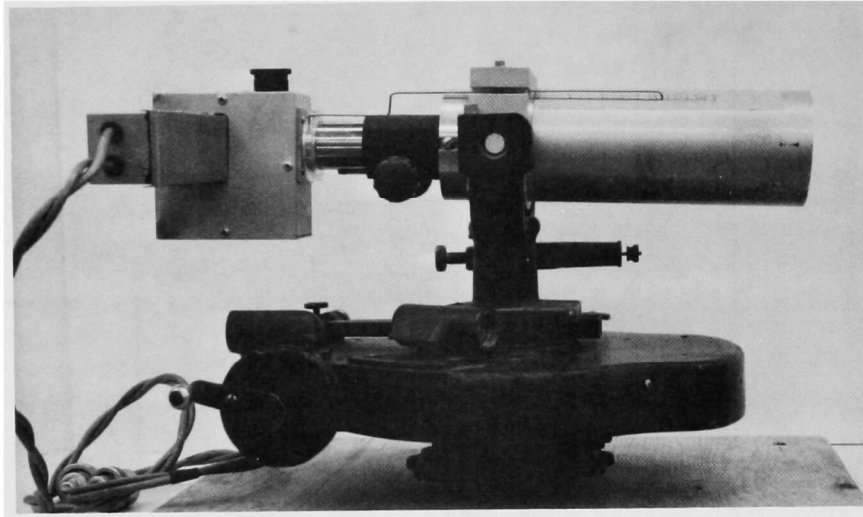


Figure 24. Photomultiplier tube and focusing telescope assembly mounted on rotating azimuth table.

photograph of Figure 24. The device is capable of fine adjustment in pointing, elevation and focus so that light scattered from a small volume at considerable distance can be made to impinge on the active surface of the 1P21 phototube. The light gathering telescope consists of a single achromat lens of 1-7/8 inch diameter and approximately 8 inch focal length. The observer's eyepiece is a 1 inch focal length lens mounted to intersect the telescope optical axis at the focal point of the objective lens. A one mm area of the mirror coating was removed at the intersection of the optical axis to form an aperture through which focused scattered light can proceed to the PMT. With this arrangement, it is thus easy to observe through the eyepiece when the detector is pointed at the desired target region of the probing gas laser beam.

From the photograph of Figure 24, it will be seen that the telescope and PMT housing are mounted in one assembly with a focusing tube arranged to provide focus range from about 4 feet to infinity. The configuration is essentially a "breadboard" design, but it proved entirely adequate for field use at the Unit 10 boiler.

Referring again to Figure 23, the output of the PMT is amplified initially with a Tektronix Model 535 oscilloscope and CA Plug-in pre-amplifier unit. From the oscilloscope, the signal is fed into the lock-in amplifier which selects and amplifies that component of the input

signal which is in phase with the 750 Hz reference signal.\* A heat-absorbing glass filter and a narrow-band dielectric interference filter placed before the telescope objective lens provide some attenuation of the background flamelight to enhance discrimination between the 0.6328 micron laser scatter and blackbody radiation of the flame. Variation in scattering intensity as a function of time is obtained by recording the coherent light signal output of the lock-in amplifier with a Brush strip chart recorder. Laboratory tests in the absence of background flamelight indicated that the full range of sensitivity for the synchronous detector system is  $3 \times 10^{-1}$  to  $5 \times 10^{-13}$  watts of chopped laser light arriving at the photo-detector. The calibration procedure is described in Section 4.

---

\* The output of the PMT could also be fed directly into the lock-in amplifier. Loss of oscilloscope power during tests at the boiler necessitated this mode of operation with an attendant reduction in signal amplification by a factor of  $\sim 10$ . The system was still adequate for the Unit 10 measurements.

## 4. RESULTS

The experimental portion of the program was divided into two distinct parts; namely, transmission and scattering measurements at the Shawnee Unit 10 boiler, and several holographic tests designed to confirm the feasibility of recording pulsed ruby laser back scatter and side (90 degree) scatter. This section of the report describes the results of both efforts. The test setup for both the transmission and scattering measurements at the Unit 10 boiler are shown schematically for reference purposes. The Unit 10 measurements and the laboratory holographic tests led to design of a three-beam holocamera for use at elevation 376 of the boiler. This design is presented and discussed as a part of the results.

### 4.1 UNIT 10 TRANSMISSION MEASUREMENTS

Laser light transmission measurements were made across the 50 foot wide Unit 10 superheater region at elevation 392. A schematic of the test setup at this elevation is shown in Figure 25. The apparatus used for transmission measurements was essentially the same as that described in Section 3.3 for the Synchronous Detector with but one exception. The focusing telescope and photomultiplier tube assembly was not used; instead, the laser beam was made to impinge directly on a silicon diode detector. A one cm<sup>2</sup> silicon diode was mounted at the focal point of a 4 inch diameter, 6 inch focal length lens. The lens and diode together with a heat absorbing (infra-red) glass filter and Wratten No. 70 red filter were assembled in an aluminum housing mounted on a tripod. The signal amplifying equipment and the chopped laser light illuminator were the same as described previously in Section 3.3.

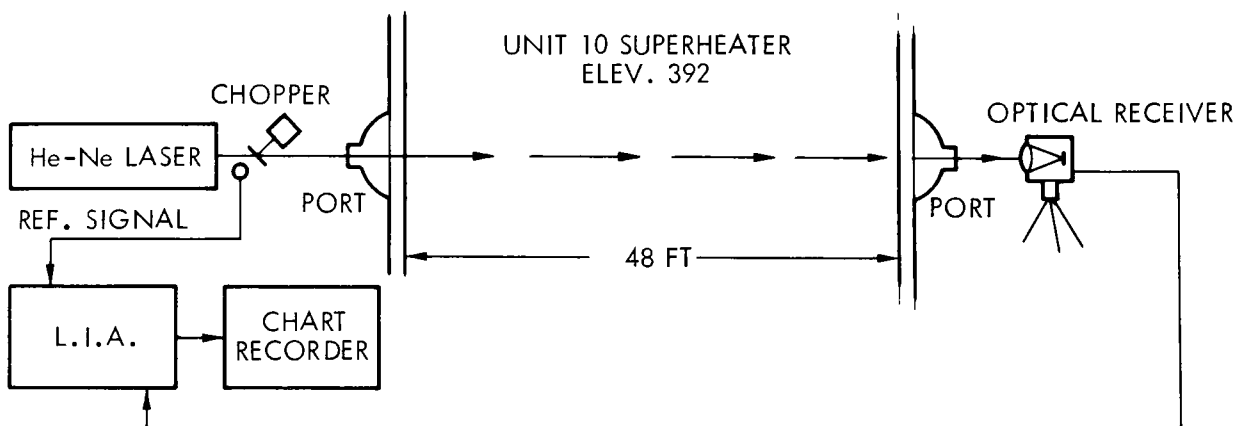


Figure 25. Schematic diagram of setup for transmission measurements at elevation 392 of the Unit 10 superheater section.



All of the transmission measurements were made in the absence of any pulverized limestone injection into the boiler. Unit 10 was operating at an electrical output of 127 megawatts during the transmission test period. At this output, the average coal feed rate was  $109.6 \times 10^3$  lb-coal/hr with a corresponding air flow of  $1 \times 10^9$  lb/hr.

Four data points were reduced from the Unit 10 superheater strip chart records. These data points were selected to obtain values of minimum and maximum light transmittance. The data are tabulated in the following table.

Table I. Transmission Measurements  
Unit 10 Superheater, Elevation 392 Ft.  
16 March 1971

Data Point	Power Received P in watts	Power Output P <sub>0</sub> in watts	Fraction Received P/P <sub>0</sub>
Minimum	$2.1 \times 10^{-6}$	.023	$9.13 \times 10^{-5}$
Maximum	$6.8 \times 10^{-6}$	.023	$2.96 \times 10^{-4}$
Minimum	$2.2 \times 10^{-6}$	.023	$9.56 \times 10^{-5}$
Maximum	$6.0 \times 10^{-6}$	.023	$2.61 \times 10^{-4}$

From these data, it will be seen that the He-Ne laser light beam attenuation varied between approximately  $1 \times 10^{-4}$  and  $3 \times 10^{-4}$  during the measurement period. The fraction  $P/P_0$ , which is the ratio of laser light received across the superheater, to the incident laser light, may be used to calculate values of the average particle number density  $n$  for each of the data points in the preceding table. This is accomplished using Eq. (2).

$$T = e^{-2n\sigma L}$$

where,

- T is the transmittance =  $P/P_0$
- e is the base of the natural system of logarithms
- n is the average number density of particles
- $\sigma$  is the average physical cross-section of the particles  
( $1.26 \times 10^{-5}$  cm)
- L is the optical path length (48 ft)

One may also calculate values of "mfp" from the transmission measurements in the superheater. These are useful for comparison with similar calculations made from the scattering data obtained at elevation 376, where straight path transmission measurements could not be made. In other words, no direct measure of the optical thickness of the boiler gases could be determined at the lower elevation thus introducing uncertainties into the particle number density calculations.

Following is a tabulation of average particle densities and mfp lengths derived from values of  $P/P_0$  in Table I using Eq. (2) and  $\text{mfp} = 1/2n\sigma$ . The average of the four measurements gives  $\text{mfp} = 66.1$  inches

Table II. Values of  $n$  and mfp for  
Transmission Data, Unit 10 Superheater  
Elevation 392 ft., 16 March 1971

Data Point	$P/P_0$	Particle Number Density		mfp	
		$\text{m/cm}^3$	$\text{n/in}^3$	Feet	Inches
Minimum	$9.13 \times 10^{-5}$	281	4612	5.16	61.9
Maximum	$2.96 \times 10^{-4}$	246	4029	5.91	70.9
Minimum	$9.56 \times 10^{-5}$	280	4589	5.19	62.2
Maximum	$2.61 \times 10^{-4}$	250	4091	5.82	69.8

#### 4.2 LIGHT SCATTERING EXPERIMENTS AT UNIT 10

In Figure 26 is a schematic diagram of the light scattering experiments performed at Unit 10 of Shawnee Power Plant, 17 and 18 March 1971. The sketch shows interconnections of equipment and the relative positions of viewing ports in the boiler wall at Plane A-A (Elevation 376). The chopped beam from the helium-neon laser was made parallel to the boiler wall at the same elevation as the centers of the viewing ports. It was then directed into one or another of the ports by a pentaprism (which has the property of maintaining a precise 90-degree angle of reflection regardless of small errors in prism rotation). The scattered light signal was measured using the synchronous detector described in Section 3.3. Two recording channels were used for recording of data. One channel was used to record an indication of flame light (total light) and one was used for the coherent detector output signal.

The first attempts to record scattered laser light were made by viewing along the inside wall of the furnace. These were unsuccessful, until it was realized that the fresh-air draft drawn into the open port was blowing all the scattering centers out of the field of view. Accordingly, a port cover was made with a 5/16" diameter hole near the center for the input laser beam to pass through. This was of thin sheet

metal, and was customarily held in place by the differential pressure between the inside and outside of the furnace. Inasmuch as the laser beam was not visible to the eye in the presence of flamelight, it was occasionally advantageous to insert a 1/4" diameter stainless steel tube through the hole in the port cover for preliminary aiming of the telescope.

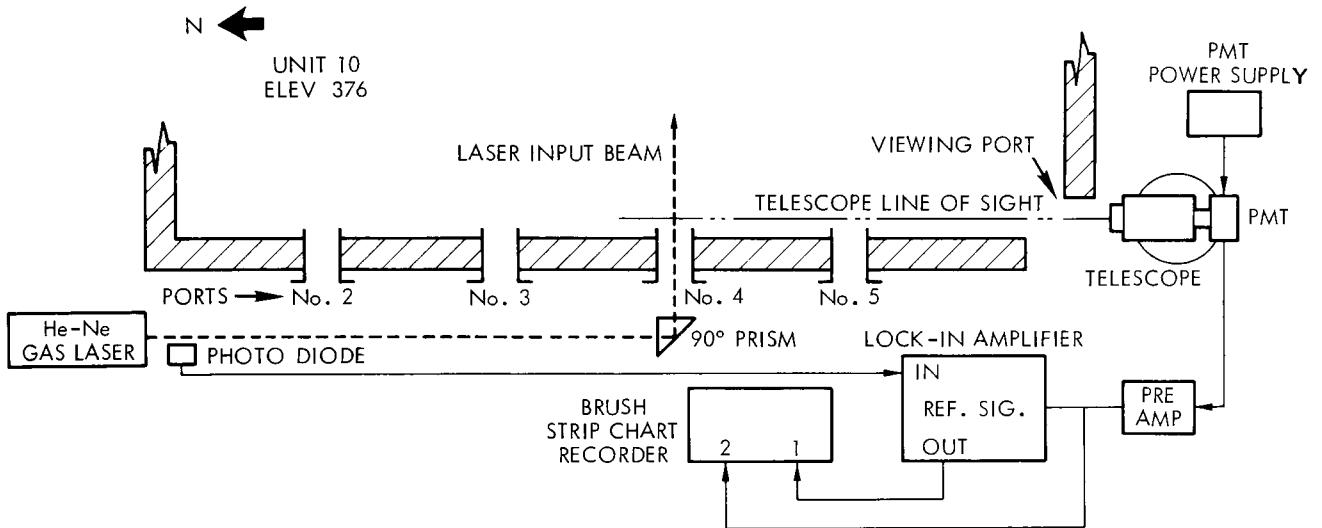


Figure 26. Schematic diagram of setup for scattering measurements at elevation 376 of Unit 10 boiler.

The calibration procedure used for this setup is described in the section immediately following. Measured results are reported and discussed in Section 4.2.

#### Calibration of Scattered Light Detector

The reference standard for power in the helium-neon laser beam is a type 401 Power Meter\*, which has a useful range of 0.1 to 100. milliwatts. This standard is applied to the synchronous detector system as follows: The laser beam is made to fall on the surface of a magnesium carbonate block placed at some convenient distance, say 20 feet, from the viewing telescope. The intensity of the beam is measured with the

\* Spectra-Physics, Inc.

power meter at the location of the block with the chopper turned off. Inasmuch as the diffuse reflectivity of magnesium carbonate is about 0.99 for light of this wavelength, it is assumed that the incident laser beam power is diffusely reflected with a consine-normal distribution, i.e.,

$$I(\theta) = \frac{p}{\pi} \cos \theta \quad (\text{watts per steradian}) \quad (7)$$

where  $p$  is the power incident on the block and  $\theta$  is the polar angle from the block normal. Now, if the angle between the telescope axis and the block normal is small, power into the telescope entrance pupil is

$$p_t = \frac{p\pi d^2}{\pi 4R^2} = \frac{pr^2}{R^2} \quad (\text{watts}) \quad (8)$$

where  $d = 2r$  is the diameter of the entrance pupil and  $R$  is the distance from the reflective block to the telescope.

With about 20 milliwatts of laser light incident on the magnesium carbonate block at about 20 feet from the telescope, a light signal is received which is several orders of magnitude stronger than scattered light signals from the experiment, but is well within the linear range of the photomultiplier tube. (This was checked over 4 orders of magnitude using neutral-density filters). Accordingly the very accurate attenuators in the pre-amplifier and the lock-in amplifier can be used to obtain a reading which corresponds to a known power arriving at the telescope.

The calibration reading thus obtained defines a calibration constant for the system which may be used during subsequent data reduction for determining the scattering ratio (more specifically, the transmittance via a particular scattering path) for a particular measurement. This is done as follows: Given a reading  $\rho$  from the lock-in amplifier ( $\rho$  goes from 0 to 1; 1 = full-scale on the meter) and an attenuation ratio (attenuator setting)  $a$  ( $1 \leq a \leq 10^\circ$ ), the calibration constant is

$$c = \frac{p_t}{\rho a} \quad (\text{watts}) \quad (9)$$

and represents the power incident on the telescope represented by a full-scale reading with maximum sensitivity. Note that the calibration power level is calculated from the dc power of the laser, while the calibration constant  $c$  is derived from the chopped light signal. The conversion from a trapezoidal wave to dc is thus accounted for, and the lock-in amplifier is effectively a "dc" power meter having a range of about  $1 \times 10^{-13}$  to  $5 \times 10^{-6}$  watts. A measurement  $p'$  is an indication of laser light power scattered into the telescope during the half-cycle of the chopper period when the light is on, and is numerically given by

$$p' = \rho a c \quad (\text{watts}) \quad (10)$$

The calibration constant thus obtained is valid for the system as long as optics remain fairly clean and the voltage on the photomultiplier is held constant. Values of  $c$  measured at Shawnee were:

$$c_1 = 1.145 \times 10^{-12} \text{ watts} \quad (\text{with pre-amp, } V_{\text{pmt}} = 600 \text{ volts})$$

$$c_2 = 7.7 \times 10^{-11} \text{ watts} \quad (\text{without pre-amp, } V_{\text{pmt}} = 700 \text{ volts})$$

### Scattered Light Measurements

Measurements were made of laser light scattered from 9 locations within the Unit 10 boiler at Plane A-A (elevation 376). The locations are shown in Figure 27. Of the 9 measurement locations, scattering from flyash only was measured at 5 points. Of these 5 points, 4 were also measured with limestone injection. In addition, measurements were made at 4 other points during limestone injection.

The 9 points are identified by numbers in Figure 27, and are also characterized by the intersections of laser beams injected through ports 2, 3, 4 and 5 with viewing telescope axis positions at scattering angles of 90, 115 and 125 degrees as shown.

Associated with each of the 9 scattering positions are two attenuation distances,  $\ell_1$  and  $\ell_2$ , together with a geometric distance  $R$ . The distance  $\ell_1$  is the distance inside the boiler to the scattering volume element. For the case of 90 degree scatter,  $\ell_1$  is essentially zero since the probing gas laser beam was parallel to the inside surface of the boiler tube wall and there was a separation of only a few inches between the wall and the beam. The distance  $\ell_2$  is that distance from the scattering volume element to the inside edge of the exit (viewing) port of the boiler. The geometric distance  $R$  is the total distance from the scattering volume to the telescope objective lens located outside the boiler. It is used in calculating the steradian correction to the measurements.\* Values for  $\ell_1$ ,  $\ell_2$  and  $R$  are given in Table III.

The fourth column in Table III is the factor  $w_\alpha$  in Equation 6, and is the effective length of laser beam in the element of scattering volume from which light is received. The values of transmittance listed in columns 5 and 6 were calculated using Equation 6 and represent the transmittance with flyash only, and with flyash-limestone mixtures, respectively.† In addition, values of the ratio of transmittance with limestone to transmittance without limestone are listed for the four points where scattering measurements were obtained for both conditions.

---

\* The diameter of the telescope entrance pupil is 1.75 inches.

† Transmittances shown in Table III are in some cases, mean values of several data points from the strip chart records.

N ←

# KEY

- 1 POINT NO LIMESTONE
- ▲ 4 POINTS WITH LIMESTONE
- 4 POINTS WITH AND WITHOUT LIMESTONE

TOTAL = 9 POINTS OF MEASUREMENT

UNIT 10  
ELEV 376

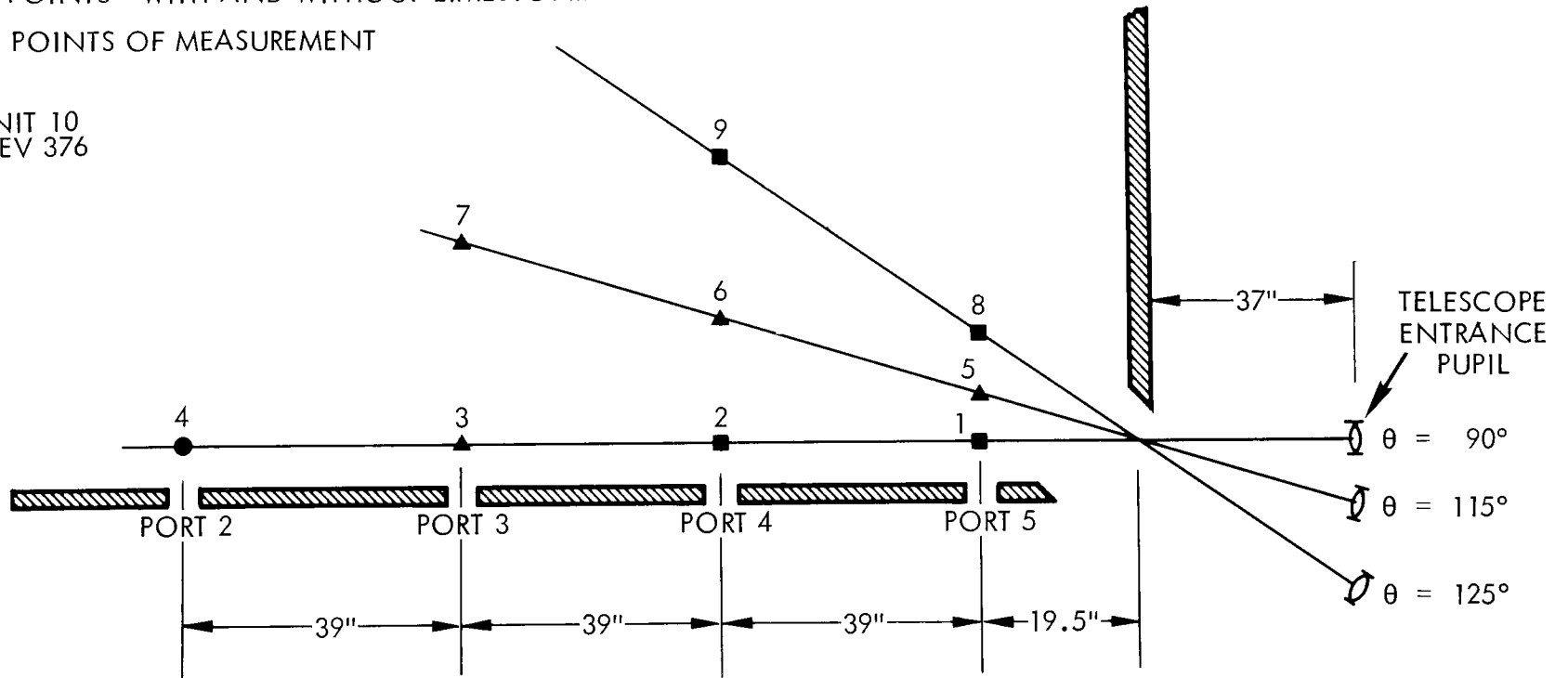


Figure 27. Relative locations from which scattered light measurements were made.

Table III.

Tabulation of results of solving Equation 6 for transmittance  
with and without limestone injection

Point No.	$l_1$ Inches	$l_2$ Inches	R Inches	$w\alpha$ Inches	Transmittance Flyash only	Transmittance Flyash + limestone	Transmittance Ratio
1	0.	19.5	56.5	.0799	$1.30 \times 10^{-8}$	$1.96 \times 10^{-8}$	1.3
2	0.	58.5	95.5	.2598	$6.0 \times 10^{-9}$	$9.89 \times 10^{-9}$	1.65
3	0.	97.5	134.5	.3858		$3.0 \times 10^{-9}$	
4	0.	136.5	173.5	.5039	$1.0 \times 10^{-9}$		
5	9.09	21.52	62.34	.1096		$1.0 \times 10^{-8}$	
6	27.28	64.55	105.37	.3228		$5.64 \times 10^{-9}$	
7	45.47	107.58	148.4	.474		$1.52 \times 10^{-9}$	
8	13.65	23.81	68.97	.1432	$6.0 \times 10^{-9}$	$1.2 \times 10^{-8}$	2.0
9	40.96	71.42	116.59	.3975	$3.0 \times 10^{-9}$	$7.2 \times 10^{-9}$	2.4

A review of the Table III data shows that for the four points from which measurements were made both with and without limestone injection, more light was received from the limestone-flyash mixture than from flyash alone. There was, however, a significant increase in fluctuations of light intensity during the limestone injection measurements.

An attempt to solve Equation 6 directly for particle number density ran into difficulties due in part to the uncertainty of the value of the scattering fraction  $\beta$ , and to the fact that a given value of the concentration function  $C$  does not yield a unique value of  $n\sigma$ . Accordingly, a "mean free path" (mfp) value of 66 inches based upon transmission measurements across the Unit 10 superheater was used with the experimental data obtained at Elevation 376 to solve for  $\beta$ . The results of these calculations are presented in Table IV.

Calculated values for the scattering fraction  $\beta$  in Table IV are given for measurements with flyash only ( $\beta_f$ ) and for those taken while limestone dust was being injected into the furnace ( $\beta_{f1}$ ). The values of  $\beta_f$  are not unreasonable, and tend to indicate some consistency in the data. The mean value is 0.358 with an uncertainty of about 30 percent. For the limestone numbers, the mean ( $\beta_{f1}$ ) is 0.571 with an uncertainty of about 60 percent, indicating either that the limestone has a different scattering fraction from the flyash, or that the assumed "mfp" was wrong.

Inasmuch as the limestone measurements were very noisy, a good probability is that one value of mfp is not correct for the entire set of measurements. For example, Table V shows the result of repeating the calculation with an input value of mfp = 55 inches. In this case, the uncertainty in  $\beta_f$  values is about the same, while the value of  $\beta_{f1}$  for point 1 is improving, it is still unreasonably high. Further, the value of  $\beta_{f1}$  for point 9 says that more light is being scattered from the intersection volume than is being received from the laser. Hence, the results are still unsatisfactory.

Another attempt was made to derive the value of  $n\sigma$  directly from the scattering measurements. For each set of measurements (with and without limestone), comparisons were made between pairs of measurements. In the ratio of two given transmission measurements, some of the factors in the basic equation cancel out (in particular, the quantity  $\beta$ ). That is,

$$\frac{T_1}{T_2} = \frac{\Gamma \frac{1}{8\pi} \frac{w_1^2 d_1}{2}}{\Gamma \frac{2}{8\pi} \frac{w_2^2 d_2}{2}} \frac{\beta f(90^\circ)}{\beta f(90^\circ)} \frac{\frac{f(\theta)}{f(90^\circ) \sin \theta}}{\frac{f(\theta)}{f(90^\circ) \sin \theta}} \frac{2n\sigma e^{-2n\sigma L_1}}{2n\sigma e^{-2n\sigma L_2}}$$

---

\* See discussion following.



Table IV  
Calculations of the Scattering Fraction  $\beta$   
Assuming mfp - 66 inches

Point No.	$\beta_f$	$\beta_f$
1	.481	.725
2	.352	.581
3	0.000	.425
4	.326	0.000
5	0.000	.389
6	0.000	.538
7	0.000	.495
8	.242	.485
9	.388	.932

Table V  
Calculations of the Scattering Fraction  $\beta$   
Assuming mfp = 55 inches

Point No.	$\beta_f$	$\beta_f$
1	.425	.641
2	.351	.578
3	0.000	.476
4	.411	0.000
5	0.000	.356
6	0.000	.592
7	0.000	.656
8	.226	.453
9	.455	1.092

whence

$$\text{mfp} = \frac{1}{2n\sigma} = \frac{L_1 L_2}{\ln \left( \frac{T_2/A_2}{T_1/A_1} \right)} \quad (11)$$

where

$$A_i = \frac{\Gamma_i w_i \alpha_i}{8\pi}$$

The results of this calculation are shown in Table VI. Here, it seems that there are a number of results which tend to cluster about some value, and a few wild results. This can be accounted for partly as follows: Equation 11 assumes that the values of  $n\sigma$  for the two measurements were the same, and therefore cancel. If this is not the case, a "wild" result can occur. If one arbitrarily ignores resultant values above 100 inches in magnitude, the two sets of results indicate a "mean free path" of about 54.6 and 54.2 inches respectively, with an uncertainty of about 33 percent. If anything, this tends to indicate that the total particulate loading (in terms of extinction coefficient per unit length) is not strongly changed during the addition of limestone dust; hence, the difference between "measured" values of  $\beta$ , with and without limestone (Tables IV and V), may indeed be due to differences between scattering properties of the flyash and limestone particles. One must regard such conclusions as tentative, in view of the sparseness of data and the simplified character of the present model.

#### Dynamic Behavior of Transmitted and Scattered Light Data

It was not an original objective of the measurements at the Shawnee Power Plant to perform a frequency-spectrum analysis of the number densities in the boiler. Nevertheless, some comments may be made on the dynamic behavior of the data, and four figures are included here as basis for such remarks. The first sample, Figure 28 is a record of the transmission measurement (no limestone injection) in the superheater region made on 16 March 1971. It is a recording of the output of the lock-in amplifier. At the left of the figure, the transmittance is fairly steady for a minute or so, then there are four cyclic variations during which the transmittance varies by almost a factor of two. The period of these variations is 30 to 35 seconds. During the course of the measurements, this phenomenon was seen to repeat itself at intervals of a few minutes. Similar cyclic bursts were later noticed on chart records in the boiler control room, suggesting that these slow oscillations may be related to the operation of some automatic control system within the boiler. For this record, the lock-in amplifier time constant was set at 0.003 second, giving a "half-power" upper cut-off frequency of about 50 Hz. Frequency components covering the range of 0.1 to about 10 Hz can be observed in the trace.

Table VI  
Calculations of the Scattering Fraction  
Using the "Two-Point" Method\*

Flyash Only		Flyash and Limestone	
Point Numbers	mfp Inches	Point Numbers	mfp Inches
1, 2	43.223	1, 2	47.963
1, 4	54.106	1, 3	45.440
1, 8	18.758	1, 5	14.027
1, 9	57.270	1, 6	51.843
2, 4	61.899	1, 7	55.512
2, 8	-381.707	1, 8	26.611
2, 9	74.888	1, 9	80.284
4, 8	82.192	2, 3	43.168
4, 9	44.615	2, 5	1320.483
8, 9	112.775	2, 6	57.262
		2, 7	59.367
		2, 8	152.185
		2, 9	156.740
		3, 5	72.349
		3, 6	17.650
		3, 7	80.604
		3, 8	57.637
		3, 9	-26.581
		5, 6	101.501
		5, 7	75.874
		5, 8	-58.478
		5, 9	224.110
		6, 7	60.579
		6, 8	75.483
		6, 9	-86.253
		7, 8	66.781
		7, 9	32.564
		8, 9	155.434

\* Equation 11

L.I.A. TIME CONSTANT = .003

1 MINUTE

WATTS X  $10^{-6}$

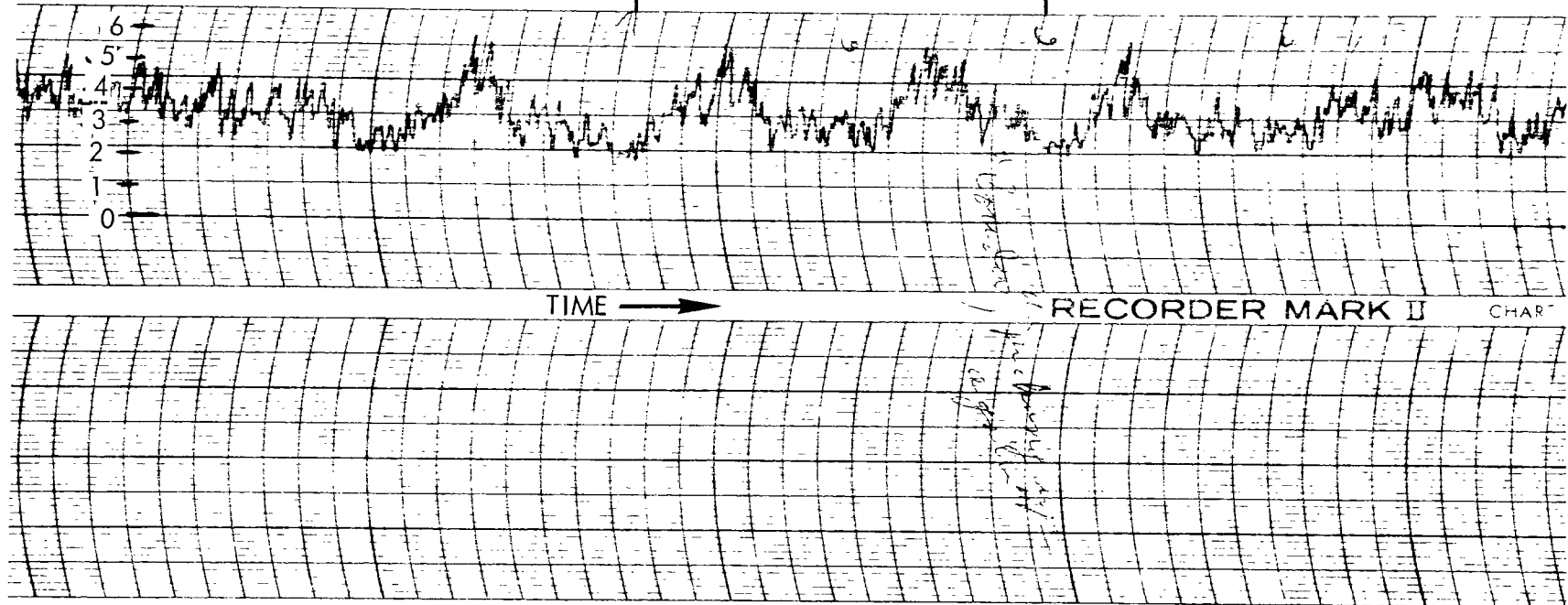


Figure 28. Strip chart record of laser light transmission across Unit 10 superheater at elevation 392, on 16 March 1971. Measurements were made in the absence of limestone injection.

An interesting record was made at the end of the experimental period (18 March 1971), as the limestone injection was being shut off. This trace is shown in Figure 29. The upper trace is lock-in amplifier output with zero at 2 major divisions from the bottom of the record. The lower trace is proportional to total light received by the phototube, zero at the top of the record. Chart speed is the same as for the previous figure. It is easy to notice, at least qualitatively, a significant difference between traces with and without limestone injection, both in amplitude and "noisiness" of the total-light and scattered-light signals.

Figure 30 is a trace made with laser light scattered from point 9 (See Figure 27) with limestone injection. For this trace, the laser beam was shuttered off, allowing the lock-in amplifier response to decay to zero. After 20 to 30 seconds it was turned on again. This was done with three different settings of the lock-in amplifier time constant in order to demonstrate the effect of this parameter on the character of the traces. With a 3 second time constant, the trace is reasonably smooth, but the decay time prevents one from obtaining a reading until about 20 seconds after a step change in input. With a time constant of 0.3 second, the circuit responds more rapidly, but noise in the trace leads to an uncertainty in the magnitude of the signal which can only be removed by taking an "eyeball average" of the signal over the subsequent period of about 20 seconds. An intermediate time constant of 0.1 second is also shown, with a similar result.

The final sample of chart records, Figure 31, was made during recording of scattered light from point 6 with limestone injection. For this trace, the recorder was allowed to run at maximum chart speed. The lock-in amplifier time constant was 0.3 second (upper cut-off about 0.5 Hz); nevertheless, frequency components up to about 70 Hz or so can be observed in the trace. Two other frequency components seem to predominate; one at about 8 - 9 Hz, and another between 16 - 20 Hz. This was about the noisiest trace recorded during the limestone injection.

No attempts were made to correlate these traces with any aspects of the limestone injection process. It seems likely, however, that the large amount of flickering of light intensity is an indication that the injection process does not result in anything like a uniform limestone density distribution. Nor does it result in a stationary distribution which could be described in a meaningful way by measurements made at one instant. This fact alone suggests that considerable improvement in the limestone process could be achieved through improvement in injector nozzle design.

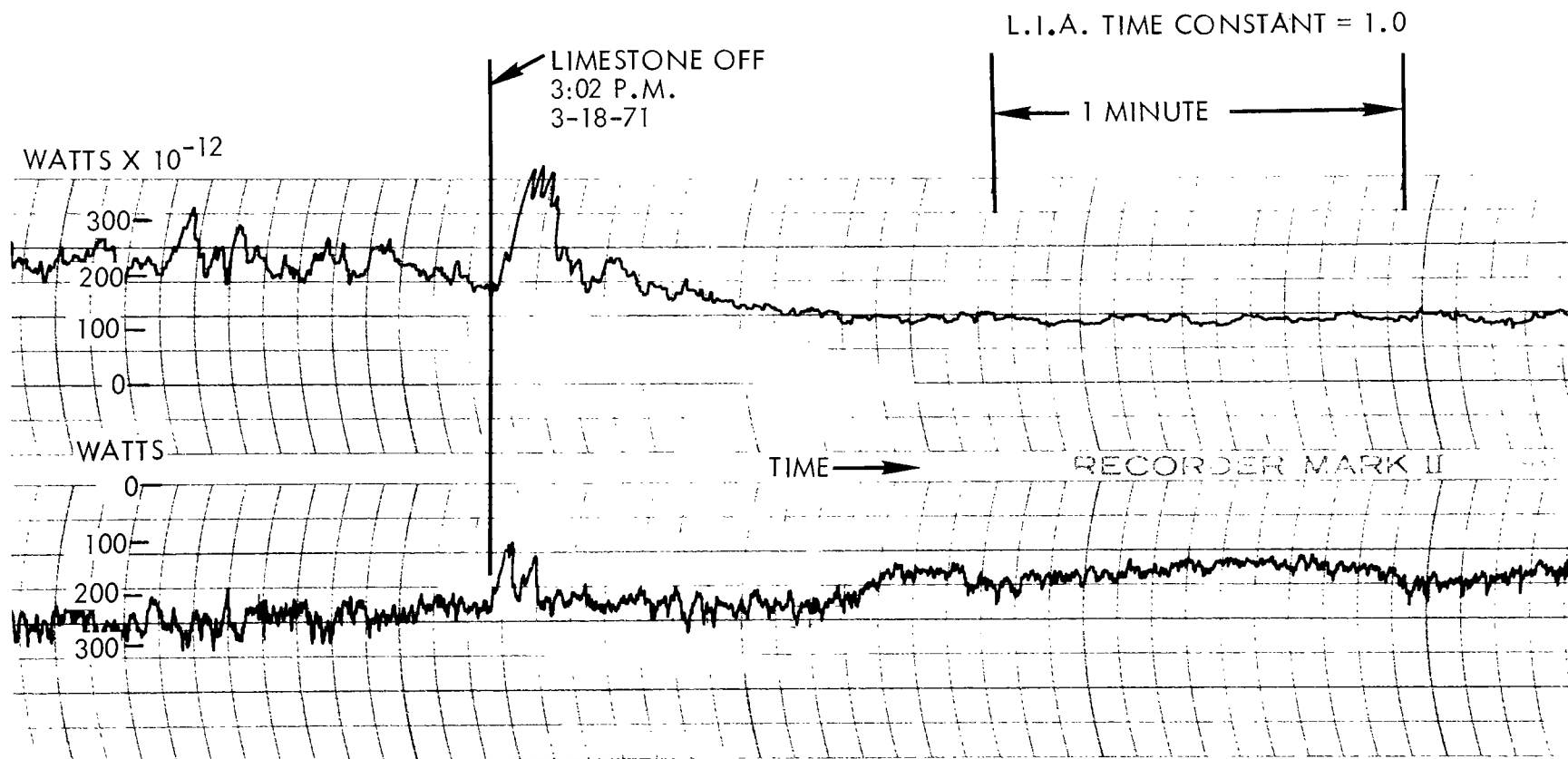


Figure 29. Strip chart record of 90 degree laser light scatter using port #5 at elevation 376, on 18 March 1971. Lower trace is proportional to total light received by PMT and thus related to combustion flamelight. Upper trace represents coherent signal from lock-in amplifier due to particulate scatter of the chopped laser input beam. The traces show the reduction in both total light and scattered light intensity as the limestone injection system was turned off.

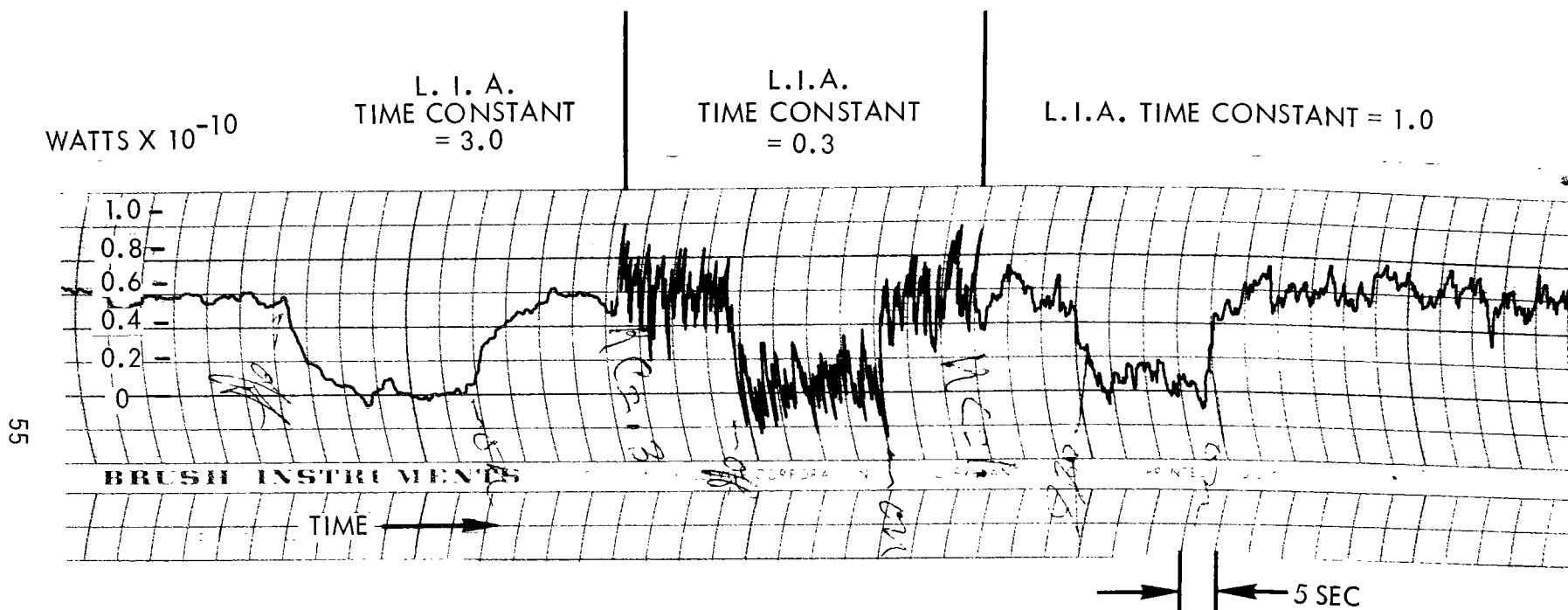


Figure 30. Strip chart record of 125 degree laser light scatter using port #4 at elevation 376, on 18 March 1971. The strip chart trace is coherent scattering signal from point 9 (see Figure 27) during limestone injection and shows the effect of different time constant settings on the lock-in amplifier.

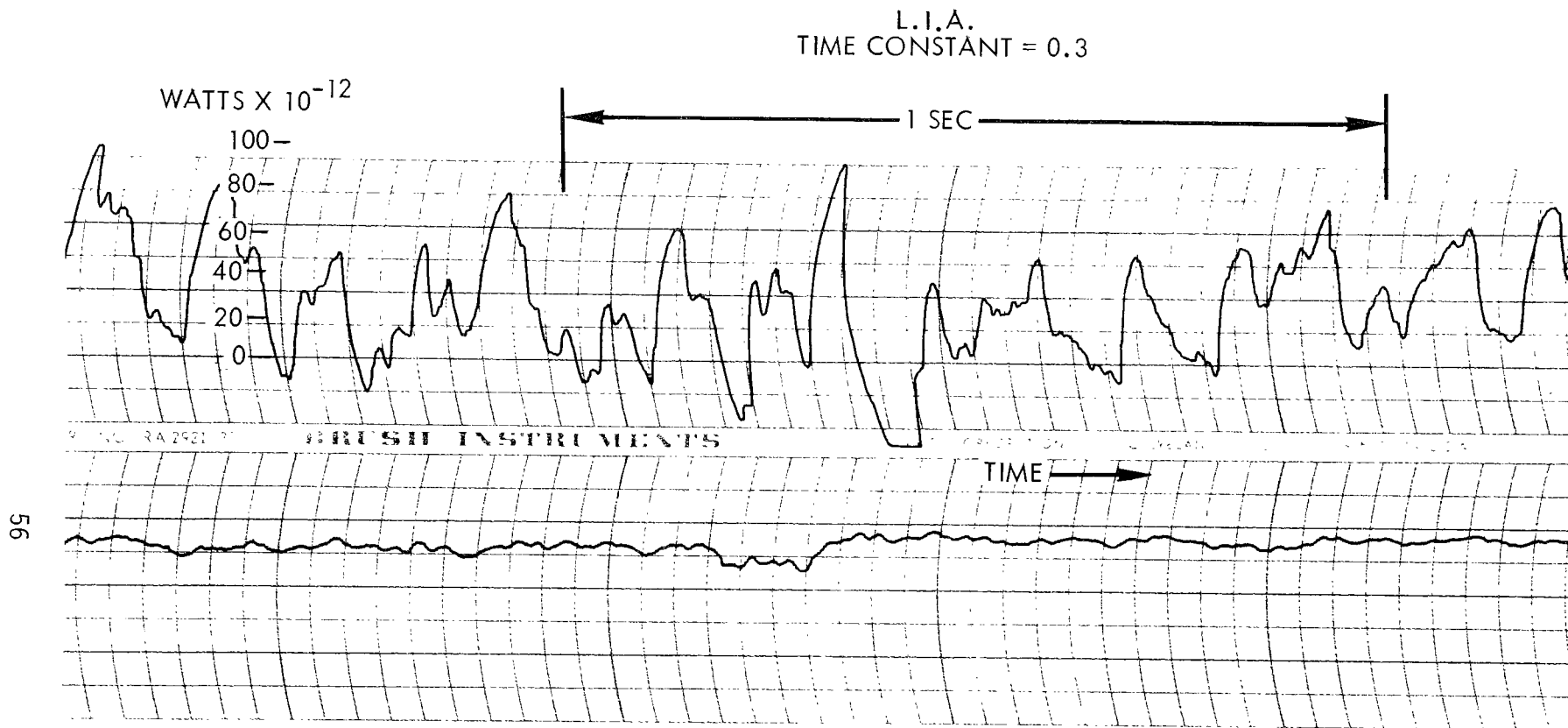


Figure 31. Strip chart record of 115 degree laser light scatter using port #3 at elevation 376, on 18 March 1971. In this example, the strip chart speed was a maximum at 125 mm/sec, with lock-in amplifier time constant at 0.3. Upper trace is coherent scattering signal. Lower trace is proportional to total light received by the PMT.



## Feasibility of Holography of Light Scattered at Large Angles

A principal objective of the experiments reported here was to determine whether meaningful holograms could be made at the same plane in the Shawnee Unit 10 boiler as was used in the scattered light measurements. Two important aspects of this question are considered here - the amount of light available in the holographic scene beam, and the possible effects of particle motion. These considerations indicate that holography may be possible at scene depths comparable to those of the present measurements. A tentative design for a holocamera setup is presented and discussed briefly. However, it is not considered possible to make a hologram which will cover the entire distance from the viewing port to a far wall.

The first aspect of the holographic process which can be examined using the scattered light data is the amount of light available in the scene beam. With Agfa 8E75 plates, a reference beam intensity of about 20 microjoules per square centimeter is typically used in order to achieve near-optimum photographic density. The required scene beam intensity may be stated in terms of a minimum scene-to-reference beam intensity ratio. A series of holograms was recently made at TRW to determine the limiting value of this quantity.<sup>7</sup> Two reference beams of equal intensity, and a scene of adjustable intensity were made to fall on the holographic plates. The beams were separated by convenient angles, and, from the viewpoint of the hologram, were derived from point sources of light. Scene to reference beam intensity ratios ranged from  $10^{-4}$  to  $10^{-7}$ . At  $10^{-6}$ , the faint point of light was barely visible to an observer viewing the reconstructed image. The point at  $10^{-7}$  intensity ratio was not visible to the eye, but could be detected with the aid of a telescope (using the light gathering ability of the larger lens).

Data from point 7 (see Table III and Figure 27) can be used as follows: The telescope entrance pupil has an area of about  $15.5 \text{ cm}^2$ , and the transmittance from point 7 was  $1.52 \times 10^{-9}$  with limestone. Accordingly, if the holographic laser pulse emits 1 joule of energy into the scattering volume, and one considers the visibility of the same scattering volume element as in the present experiment, the scene-to-reference beam intensity ratio is

$$\frac{1. \times 1.52(10)^{-9}}{15.5 \times 20(10)^{-6}} = 4.5 \times 10^{-6}$$

which is near the lower limit of the range. This estimate considers only the visibility of one small volume element; hopefully, the hologram will show scattered light from a great many such elements covering several feet of the incident laser beam.

The other aspect of the problem is the possible effects of particle velocity on visibility in the holographic image. A commonly used criterion says that to make a good hologram, the object should not move during the laser pulse such as to cause a path length change of more than  $1/10$  wavelength in the scene beam. Slight departure from this criterion will not necessarily cause complete failure of the holographic process, although unpredictable changes in visibility may result. Without going through all the details of the analysis, one may observe that the direction of particle velocity is of crucial importance, and that a velocity component greater than about 3 meters per second in an adverse direction may make a scattering particle invisible in the hologram. However, if the velocity components greater than this magnitude are in a direction perpendicular to the plane containing both the incident and received beams, particle visibility may not be impaired. We have the favorable result, also, that scattered light holograms have been successfully made in the Unit 10 boiler. However, we note that plane A-A has a narrower cross section than the plane at which holograms were previously made, and that curvatures in the flow (due to flow around the "nose" of the superheater) and turbulence could cause erroneous variations in image intensity.

The schematic diagram of Figure 32 shows a proposed holocamera design for recording side scatter of a ruby laser beam by particulate in the Shawnee Unit 10 boiler at elevation 376. Arrangement of the holocamera optics makes use of existing boiler ports at this elevation.

The incident ruby scene beam enters the boiler through one of the existing four ports on the west side of the boiler. The incident beam is shown as an unexpanded collimated beam; however, the addition of a cylinder lens at the entrance to the boiler port would permit the fanning of the incident beam within the geometric limitations of the port.\* Scattering of the incident beam is received by the hologram through the large port on the southwest corner of the boiler.

The reference beam is formed using a wedge and telescope arrangement. The reference beam is expanded and collimated to a 5-inch diameter, and directed parallel to the outside of the west wall of the boiler. A large wedge divides the primary reference beam into two components. Front surface mirrors are used to recombine the two reference beam components at the plane of the holographic plate. The result is a three-beam holocamera similar to that demonstrated in the laboratory.<sup>2</sup> The addition of the second reference beam enables the reconstruction process to be linearized and provides the sensitivity necessary to record very weak scene intensities.

---

\* Refer to the results of the low angle forward scattering holograms recorded previously at elevation 365 for examples of recordings with fanned scene beams (Reference 1).

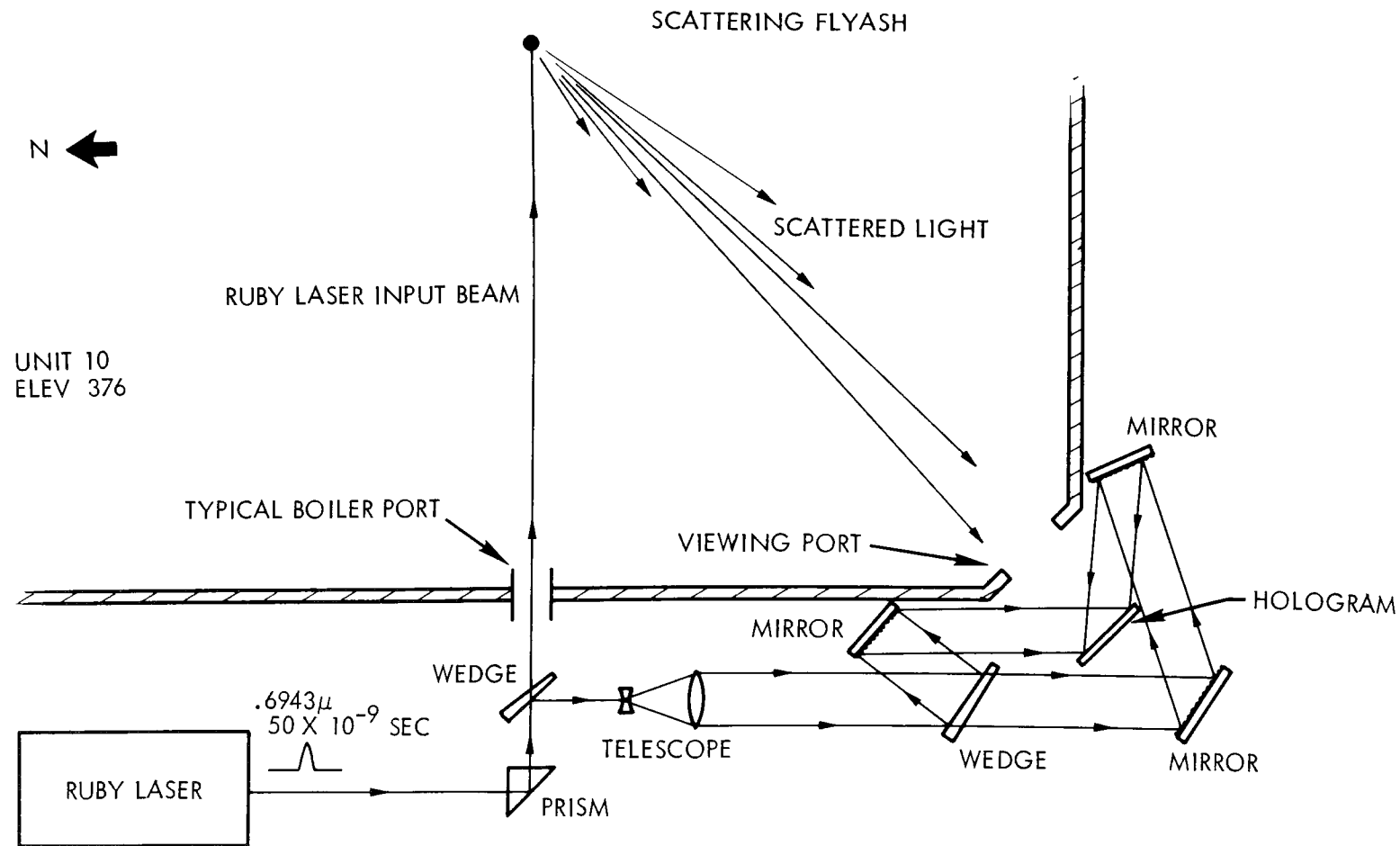


Figure 32. Schematic diagram of proposed three-beam ruby laser holocamera for use at the Shawnee Unit 10 boiler to record side scattering. With modification, same apparatus could be adapted to record back scatter.

## 5. CONCLUSIONS

From the scattering analysis, laboratory tests and measurements made at the Shawnee Unit 10 boiler, the following conclusions have been reached concerning each of the following topics:

### Holography of Scattered Light

- The holography of back scatter and side scatter is feasible. Recordings were made in the laboratory of static scenes and aerosols to demonstrate this feasibility.
- The holography of side scatter and back scatter by particulates in the boiler is possible. This is based upon scattering measurements made with the synchronous detector at elevation 376 in the boiler. Demonstration of feasibility remains to be verified by test at the boiler. Uncertainties with respect to particle velocity components and actual scene-reference ratios prevent a definite conclusion by analysis only.
- Of the two alternative methods considered during the present work, side scatter holography and back scatter holography, the latter appears to offer the most promise. This is based on the fact that laboratory tests indicated a factor of ~20 increase in the amount of light scattered in the backward direction, over that scattered in the 90 degree to 125 degree side scattering directions.
- Both the side scattering and back scattering techniques suffer limitations with regard to particle velocity components due to turbulence, etc. Velocity limitations for both techniques are about the same (around 1 to 3 meters/sec).
- Based upon all of the past and present scattered light holography studies, the forward scattering method is by far the optimum method for visualizing particle distributions and acquiring particle density data. In addition to being previously demonstrated at the boiler, the holography of low angle forward scatter has two distinct advantages; namely, it is relatively insensitive to particle velocities, and more favorable scene-to-reference beam ratios result since particle scattering intensity is predominantly in the forward direction.

### Acquisition of Particle Density from Scattering Measurements

- Straight path transmission measurements at elevation 392 of the superheater indicated that particle densities ranged between 4000 and 4600 flyash particles/in<sup>3</sup> in the absence of limestone dust injection into the boiler.

- Comparative tests at elevation 376 showed that there was an increase in scattered light intensity of between 1.3 and 2.4 during periods of limestone dust injection. Strip chart traces exhibited considerable amounts of "noise".
- Direct solution of the particle scattering model proved impractical. This was due to uncertainties concerning the scattering fraction  $\beta$ , and the fact that given values of the concentration function ( $2n\sigma L e^{-2n\sigma L}$ ) did not result in unique values of  $n\sigma$ .
- The alternate "two point" method of deriving  $n\sigma$  from the scattering measurements did not demonstrate a sensitivity to increases in particle density due to the presence of limestone dust. Tentatively, it is concluded that the attenuation coefficient per unit length ( $2n\sigma$ ) is not significantly changed at Plane A-A. Stated another way, changes in the attenuation coefficient are within the "noise level" of the scattering intensity measurements.
- A partial reason for the apparent lack of change in the attenuation coefficient may be due to the particle encapsulation phenomenon noted during the scanning electron beam microscopy studies.
- The concentration function  $y = xe^{-x}$  places a limit on the distance into the boiler particle flow field which may be interrogated via back scattering measurements. At Plane A-A, the characteristic distance was approximately 6 feet inside the boiler volume.

#### Particle Flow Field Dynamic Characteristics.

- Limestone particle distribution at Plane A-A does not appear spatially uniform nor is the distribution constant or repetitive with time, based upon the apparently random intensity and frequency variations of the strip chart records.
- The frequency characteristics of the transmitted and scattered light strip chart traces vary randomly and range from about 0.1 to 10 Hz in the absence of limestone injection.
- During limestone injection, the degree of "noise" increased. Frequency components up to about 70 Hz were observed. Two frequencies appeared to predominate; one at 8 - 9 Hz, and another at between 16 and 20 Hz.

- Occasionally, definite repetitive cyclical variations did occur. In one example, the period of these variations was approximately 30 to 35 seconds. It was tentatively concluded that these slow oscillations correlate with some automatic control system associated with the operation of the boiler.

## 6. RECOMMENDATIONS

It is recommended that the method of low angle forward scatter holography be utilized to investigate and optimize limestone dust distribution in the Shawnee Unit 10 boiler. A laser-illuminated synchronous detector would be used in conjunction with holography to provide a continuous monitor of localized dust concentrations. The synchronous detector would be a part of the holocamera setup and provide complimentary data to the instantaneous holographic records. The output of the detector should also be integrated into the overall data acquisition system for the dry limestone injection apparatus and boiler operation.

It is recognized that the utilization of forward scattering (transmission) holography will necessitate cutting additional ports in the boiler; however, the capability of making in situ detailed measurements (instantaneous and continuous real time) of particle number density distributions as a function of limestone injection variables would aid in the development of the dry limestone system.

## REFERENCES

1. B. J. Matthews and R. F. Kemp, "Holographic Determination of Injected Limestone Distribution in Unit 10 of the Shawnee Power Plant," TRW Report No. 14103-6001-R0-00, June 1970.
2. B. J. Matthews and R. F. Kemp, "Investigation of Scattered Light Holography of Aerosols and Data Reduction Techniques," TRW Report No. 14103-6002-R0-00, November 1970
3. Private communication from D. T. Clay, 17 March 1970. See also Tennessee Valley Authority Report No. 54 covering particle size analysis of limestone and flyash during period of 9 July - 6 August of 1969.
4. G. H. McClellan, "Physical Characteristics of Calcined and Sulfated Limestones," Paper presented at the NAPCA Symposium on the Dry Limestone Injection Process, Gilbertsville, Kentucky, June 1970.
5. Walter C. McCrone in: Air Pollution, Vol. II, by Arthur C. Stern (Academic Press, New York) 1968.
6. R. F. Wuerker and L. O. Heflinger, "Laser Holography Study," Interim Report, Air Force Avionics Laboratory Report No. AFAL-TR-70-178, January 1971.
7. L. O. Heflinger and R. E. Brooks, "Holographic Instrumentation Studies," TRW Systems Report No. 12122-6007-R0-00, prepared for NASA Ames Research Center under contract NAS2-4992, December 1970.